Technical University of Denmark

Kim Kofoed Nielsen (s103624)

Modelling and Control of Float Zone Silicon crystal growth

Master's Thesis, February 2017

DTU Compute
Department of Applied Mathematics and Computer Science

KIM KOFOED NIELSEN (S103624)

Modelling and Control of Float Zone Silicon crystal growth

Master's Thesis, February 2017

Supervisors:

Niels Kjølstad Poulsen, Associate Professor at the Department of Applied Mathematics and Computer Science of DTU

John Bagterp Jørgensen, Associate Professor at the Department of Applied Mathematics and Computer Science of DTU

Dr.-ing **Nico Werner**, Project Manager at Topsil GlobalWafers A/S

Nicolai Hanssing, M.Sc. Control Engineering & Automation at Topsil GlobalWafers A/S

DTU - Technical University of Denmark, Kgs. Lyngby - 2017

Modelling and Control of Float Zone Silicon crystal growth

This report was prepared by:
Kim Kofoed Nielsen (s103624)

Advisors:
Niels Kjølstad Poulsen, Associate Professor at the Department of Applied Mathematics and Computer Science of DTU
John Bagterp Jørgensen, Associate Professor at the Department of Applied Mathematics and Computer Science of DTU
Dr.-ing **Nico Werner**, Project Manager at Topsil GlobalWafers A/S
Nicolai Hanssing, M.Sc. Control Engineering & Automation at Topsil GlobalWafers A/S

DTU Compute
Applied Mathematics and Computer Science
Richard Petersens Plads, building 324
2800 Kongens Lyngby, Denmark
Phone +45 4525 3031
compute@compute.dtu.dk
www.compute.dtu.dk

compute@compute.dtu.dk

Project period: August 2016- February 2017

ECTS: 32.5

Education: MSc

Field: Electrical Engineering

Class: Not confidential

Remarks: This report is submitted as partial fulfilment of the requirements for graduation in the above education at the Technical University of Denmark.

Table of Contents

Abstract

This thesis deals with the application of offset free control, using a model predictive controller, on the process of producing silicon wafers operating in a stable state subject to unknown disturbances. Because of the disturbances the process would experience offset errors in the outputs.

A linear model was derived from a non-linear model developed through the work of Nico Werner in his PhD thesis. The model was then analysed to verify that it could be used as a basis for the model predictive control. A simple disturbance model used in the estimation of the unknown disturbances and used in the control to achieve offset free control.

The control solution was implemented and simulated in MATLAB, excited by different disturbances and evaluated, with respect to the controllers ability to keep the controlled outputs at their steady states.

The results showed that the controller was able to control and track reference changes to the system. They also showed that it could remove offset errors in the crystal diameter, with a small offset in the the lower zone height. This is due to the uncontrollable marginally stable poles in the system.

Preface

This thesis was prepared as a collaboration between academia and industry. The university partner was the Department of Applied Mathematics and Computer Science (DTU Compute) and Topsil GlobalWafers A/S, in partial fulfilment of the requirements for receiving the master degree in Electrical engineering degree with specialization in Automation and Robot Technology. A big thanks to my supervisors, both partners was a great pillars of support during the projekt. Also a thanks to my friends for support in the last hours.

The work in this thesis was carried out from August 2016 to February 2017. This project was supervised by

- **Niels Kjølstad Poulsen**, Associate Professor at the Department of Applied Mathematics and Computer Science of DTU
  John Bagterp Jørgensen, Associate Professor at the Department of Applied Mathematics and Computer Science of DTU
  Dr.-ing **Nico Werner**, Project Manager at Topsil GlobalWafers A/S
  Nicolai Hanssing, M.Sc. Control Engineering & Automation at Topsil GlobalWafers A/S

Kim Kofoed Nielsen (s103624) February 2017

CHAPTER 1

Introduction

1.1 Motivation

The motivation for this thesis work is both practical and academic. Topsil GlobalWafers A/S is looking into using linear models for their control scheme and gain an insight into using offset free control. The presented work successfully investigates linear control methods, and linear offset estimation, for possible future implementation at Topsil GlobalWafers A/S.

Topsil GlobalWafers A/S is a supplier of ultra pure silicon to the semiconductor industry. They produce custom made silicon wafers, which are placed under strict requirements with respect to the crystal properties. The silicon is produced by melting raw polycrystalline silicon crystals and regrowing it into a refined monocrystalline silicon crystal using a seeding crystal[1]. This process happens in a pressurised chamber that needs to be both automatically controlled by a computer and supervised by an operator. Currently, the implemented controller used in their process is based on the non-linear model designed by Nico Werner, through his PhD work at IKZ[1] and later work at Topsil GlobalWafers A/S, which is using a constrained model predictive control to grow the silicon crystal, that replaced conventional PID controllers. It showed significant improvement of the yield in the produced crystals and it reduced the workload for the operators.

The research is new focusing on two areas of the current setup, one is the use of a linear model, the other is offset free control. The model is based on complex non-linear mathematics, that not every technician or engineer that has to maintain the system can understand. The mathematical techniques for non-linear models are more rigorous and much less general. They want to find out if a linear model is able to provide the same prediction accuracy as the non-linear model for their control system. It is common knowledge that control designers use a linear model when possible, and only deviate from this when the non-linearities cannot be controlled through linear control methods. The linear model analysis techniques are also more general, easy to understand and use. Hence a linear state space model is developed and analysed in this thesis.

[1] This process is further explained in the chapter: Introduction

A disadvantage is that the controller used does not take into account unknown disturbances, that causes an offset error on the size of the produced silicon crystal, reducing the potential yield. These disturbances can be caused by actuator errors, sensor errors, mismatch in the model and external disturbances and they are not directly measurable. There is a lot of research on the topic of offset control for linear models, with such work covered in [2], [3], [4], [5], [6]. Unknown disturbance cannot be directly measured by sensors, they can however, be can be detected indirectly by estimators. With the combination of a linear model based predictive controller and a state estimator such as a Kalman filter, the disturbances can be estimated and rejected by the controller. The model predictive controller is chosen because multiple inputs and multiple output problems are handled naturally, and the limitations and boundaries of a process can be respected. By using a linear model of the system the Kalman filter can remove the noise from the measurements and estimate both the real values of the measurements and the real values of the disturbances. When the disturbances have been estimated it is relatively straightforward to remove their effect on the process and achieve zero offsets.

1.2 Process Introduction

Topsil GlobalWafers A/S is a global supplier of Ultrapure silicon wafers. Silicon is mostly used in electronics. Examples include integrated circuits, detector and sensor devices, MEMS fabrication, optoelectronic components, and solar cells. Ultra pure silicon wafers are mainly used for high-power electronics because they require very specific material characteristics, such as homogeneous resistivity, which is the property that quantifies how the flow of the electrical current is opposed. A low resistivity means that the electricity can flow more easily through the material. [7]

At Topsil GlobalWafers A/S they use the Float Zone (FZ) technique, a contact-less inductive heating growing method using a float zone machine. This method is required for ultra pure crystal growth, as the silicon does not come in contact with any contaminating surfaces during the process. For this reason, the produced silicon crystals achieve a much higher purity than the traditional Czochralski (CZ) method. The CZ method uses a crucible to contain and heat the polycrystalline silicon.

A float zone machine consists of a pressurized chamber, which is equipped with inductive coil and is filled with gas that is inert to silicon[8], and two spindles, one on the top of the chamber which holds the polycrystalline silicon to be melted and one at the bottom, holding the seeding crystal from which the monocrystalline silicon is to be grown. The coil emits a radio frequency magnetic field which is controlled by a generator, and the pistons are able to rotate and push and pull the crystals.

The float zone process can be divided into seven chronological phases. The following is a summary of the basic process steps. See [8] are more detailed explanation.

Figure 1.1: Image of the production hall at Topsil GlobalWafers A/S. To the left is shown a float zone machine in an open position. In the green boxes are the crystal holders that contains and pulls the silicon. In the red box is the pressurised chamber. When used in production, the two holders locked into the chamber and sealed.

- *Growing the feed tip*
  This is the preparation step to produce suitable conditions for creating the thin neck. With the magnetic field the tip of the polycrystal is melted off. The seed crystal is moved upwards into the molten drop of the polycrystal to form the feed tip. When the feed tip has been established the process moves on to the thin neck phase.

- *Growing the thin neck*
  The seed crystal is moved downward with a relatively high pull rate, creating a thin neck. The necking process is necessary to create a dislocation-free crystal, before the cone phase. Here the diameter of the monocrystal is reduced from the seed crystal size of about 5 mm to 2-3 mm. This is done to remove dislocations in the crystal [9]. The crystal is now ready to be grown to the full diameter.

- *Creating the molten zone*
  The area of the molten zone is expanded such that the crystal can start to increase in diameter. Notably in this phase, the pull rates of the pistons are kept constant, and the molten zone is adjusted with the heater power to stabilise it.

- *Growing the cone shape*
  In this phase, the crystal is increased in diameter creating a cone. It is controlled by changing the heater power and the pull rate of the feed crystal.

- *Landing*
  The landing is the phase where the crystal shape is changed from a cone to a cylinder. The desired diameter of the crystal has been reached.

- *Growing the cylinder*
  This is the phase where the crystal diameter is kept constant. The pull rates and the heater power is also kept constant. This part of the process in a stable state. At this state the process is in a stable state, and it is from this portion of the crystal that is used for wafers.

- *Closing the crystal*
  When the feed crystal is about to be completely melted, the heater power is adjusted to compensate for the heat transport effect that occurs due to the reduced length. In this phase, it is important not to close the crystal too quickly as there is a bowl of molten material in the crystal. If this bowl is encapsulated in the crystal without allowed cooling, it can cause a fracture in crystal, and effectively breaking the crystal and equipment as liquid silicon leaks out. When the crystal has successfully been closed, the process ends, and the new monocrystallize silicon is brought to post processing.

Figure 1.2 shows the inside of the pressurised chamber. Here the process is in the growth phase "Growing the cylinder". A clear picture of the molten zone can be seen (the bright yellow zone), flowing from the top crystal through the eye of the coil and unto the growing crystal. The line dividing bright yellow zone and the orange zone is called the melting line. The material below is heated liquid silicon. The crystallisation line cannot be seen in this picture as it is obfuscated by the machine.

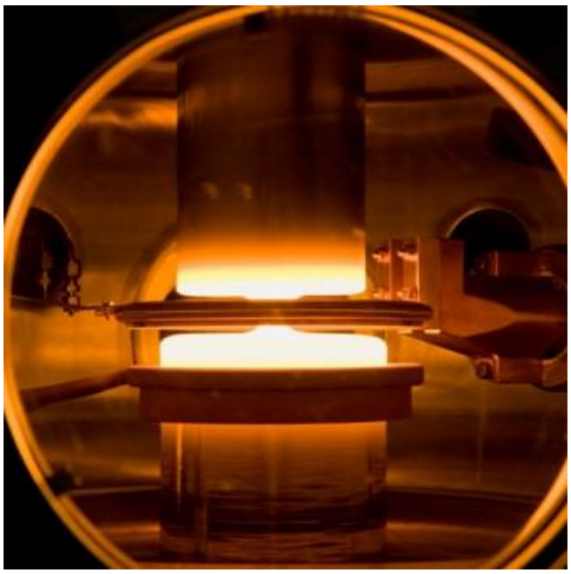

Figure 1.2: Inside the pressurised chamber.

Figure 1.3 shows a finished silicon ingot ready to be cut into wafers. The left part of the crystal shows the cone phase, where the diameter is increased to the desired size and the right, shows the cylinder phase where the diameter is kept constants.

Figure 1.3: Finished Silicon ingot.

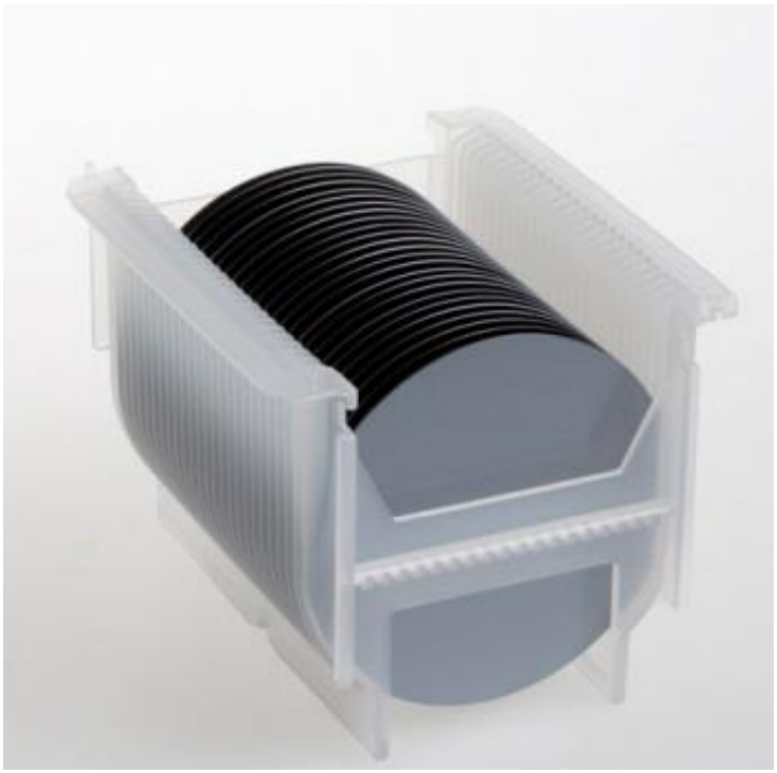

Figure 1.4: A picture of finished and cut silicon wafers.

The finished product is thin silicon wafers which are shown in figure 1.4. These wafers are ready to be made into high-efficiency semiconductor devices.

1.3 Thesis scope

This master thesis is the final part of the master's degree in Automation and Robot technology at the Technical University of Denmark, showing the accumulated skills and knowledge of the student. The objectives of this project are to investigate the possibility of using linear models for control of the float zone process. As control design of non-linear models are complex and control design with linear models is a well researched area. However, non-linear model based controllers are

more likely to be able to control the system with a better performance. Therefore an analysis of the linear model must be conducted such that it can be shown that it is able to calculate a accurate approximation of the response of the non-linear model. Finally a offset free controller will be designed, such that any model mismatch or disturbance that causes offset errors in the crystal diameter can be removed.

The main objectives of this thesis are to:

- Apply linear modelling techniques to the non-linear differential equations.
- Validate the linear model by calculating the approximation errors.
- Analyse of the linear model.
- Design a Model Predictive Controller.
- Design an Observer with disturbance estimation to achieve offset free control.
- Run simulated tests of the controlled process under disturbances.

The linear model will be based on the non-linear model from the PhD work of Nico Werner [1].

CHAPTER 2

The Float Zone Process Model

This chapter presents a model for the float zone process. The equations and model parameters have been derived and identified in the PhD thesis of Nico Werner [1]. The model is based on physical conservation laws, such as energy and mass balances. This section gives a summary of the non-linear differential equations from [1], which are describing the dynamical behaviour of the float zone process.

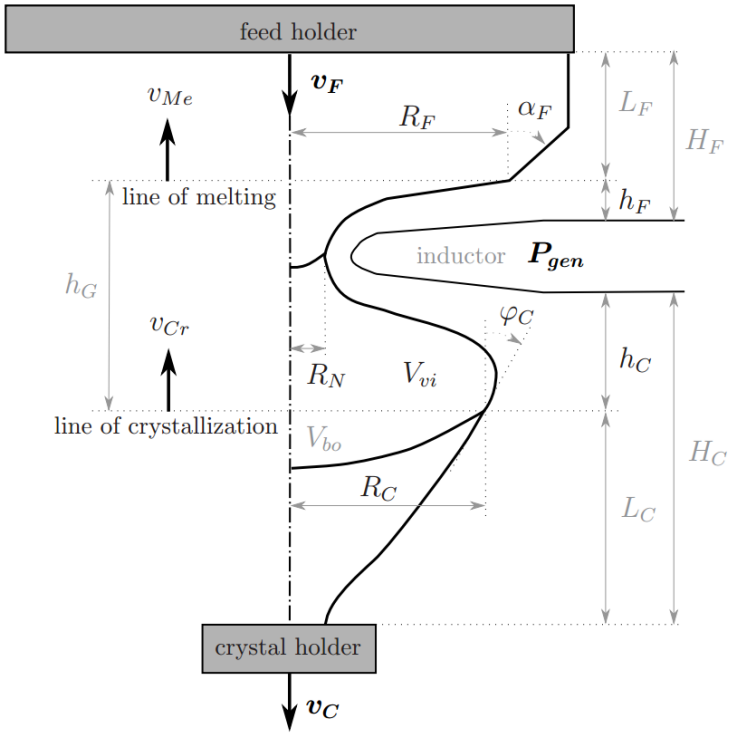

Figure 2.1: Sketch of the float zone process in the cone phase (From [1]). Shown are the state, input and auxiliary variables

Figure 2.1 shows a cross section sketch of the float zone process in the cone phase. The poly-crystalline silicon is placed in the feed holder and the mono-crystalline silicon is held in the crystal holder. From this point, the mono-crystalline silicon will be called the 'crystal' and the

polycrystalline silicon will be called the feed or feed crystal. The table 2.1 shows the variables of the process and their respective units.
The adjustable variables in the process are the generator power P_{gen}, the pull rates of the feed holder v_F and the crystal holder v_C. There is also a rotation around the length of the crystal rods, however, these rotations are not modelled.

The solid feed crystal is molten off by inductive heating, which causes the molten material to flow from the feed crystal through the inductor hole on top of the solidifying crystal. The total melt volume V_{tot} consists of multiple parts: (a) The visible part V_{vi}, (b) the volume of the melt bowl V_{bo} which is hidden in the crystal, and (c) a volume which is covered by the inductor. Part (c) is assumed to be constant and it is not considered in the process dynamics [1]

The melting rate is determined by the negative change of the feed crystal length L_F with respect to the melting line and the feed holder. The melting line is the horizontal line dividing the melting front from the solid material. The crystallisation rate is determined by the change in the crystal length L_C with respect to the crystallisation line and the crystal holder. The crystallisation line is the horizontal line that divides the crystallised solid from the melt. A positive melting rate gives a decreasing feed crystal length and a positive crystallisation rate gives an increasing crystal length. The angle of the feed crystal α_F is the measured directly above the melting line with respect to the vertical axis and the angle of the crystal ϕ_C is measured on the line of crystallisation.

Variable	unit	Note
R_C	[mm]	Radius of the monocrystal
R_F	[mm]	Radius of the poly crystal
h_C	[mm]	Distance from the crystallization line to the inductor bottom
h_F	[mm]	Disturbance from the melting line to the inductor top
D_C	[mm]	Diameter of the monocrystal
D_F	[mm]	Diameter of the feed crystal
V_{vi}	[cm^3]	Volume of the visible melt.
V_{bo}	[cm^3]	Volume of the hidden melt bowl
V_{Fr}	[cm^3]	Volume of the hidden solid feed residual
U_{gen}	[kV]	Adjustable generator voltage
U_{ind}	[kV]	The voltage in the inductor coil
P_{gen}	[kW]	Generator power
P_{ind}	[kW]	The Power output of the inductor coil
v_{Cr}	[mm/min]	The rate of crystallization in the monocrystal
v_{Me}	[mm/min]	The rate of melting in the feed crystal
v_C	[mm/min]	The adjustable pull rate of the crystal holder
v_F	[mm/min]	The adjustable pull rate of the feed holder

Table 2.1: Table of variables and their respective units.

The upper zone height h_F is the height between the upper edge of the inductor and the melting line and the lower zone height h_C is the height between the lower edge of the inductor and the

crystallisation line.

The size of the produced monocrystalline rod is measured in diameter D_C, however, the model uses its radius R_C. In short, both are used to describe the same thing. The size of the monocrystalline rod is determined by the angle ϕ_C at the crystallisation line as seen in sub figure 2.2b. The size of the diameter poly-crystalline rod is predetermined, however, its radius R_F is used in the model to determine the dynamics of the melt volume.

2.1 Non-Linear Model equations

In this section, the non-linear differential equations of the FZ process are presented. They are modelled in Werner [1].

2.1.1 Angle of the Feed rod

The angle of the feed rod α_F is used to determine the radius of the feed crystal. In this project, the change in the angle is assumed to be constant.

$$\frac{d}{dt}(\alpha_F) = 0 \tag{2.1}$$

2.1.2 Radius of feed and crystal rods

The differential equations for feed radius R_F and crystal radius R_C are described using the relationships according to the triangle in figure 2.2a.

$$\mathrm{d}R_F/\mathrm{d}L_F = -\tan(\alpha_F) \tag{2.2}$$

where the change in the length of the feed rod can be described as the melting rate The melting rate can be described as the change in length of feed rod

$$v_{Me} = -\frac{d}{dt}(L_F) \tag{2.3}$$

The crystallization rate can be described as the change in the length of the crystal rod

$$v_{Cr} = \frac{d}{dt}(L_C) \tag{2.4}$$

and equation 2.3 leads to the following differential equation for the radius of the feed rod

$$\frac{d}{dt}(R_F) = v_{Me}\tan(\alpha_F) \tag{2.5}$$

in which α_F is the angle of the feed rod. Following the same relationship rule in figure 3.2(b) in [1], with respect to the crystal rod

$$\frac{d}{dt}(R_C) = v_{Cr}\tan(\phi_C) \tag{2.6}$$

where ϕ_C is the angle of the crystal rod at the crystallization line.

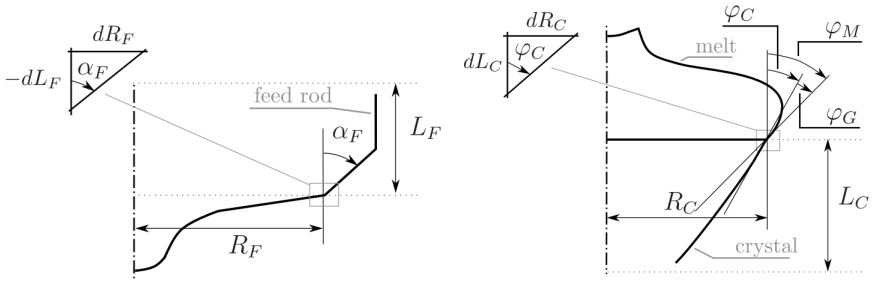

(a) (b)

Figure 2.2: From [1].

2.1.3 Heights of the upper and lower zone

The zone heights is where the input variables creates a relation to the other state variables. The upper zone height as show in figure 2.1 is given by

$$h_F = H_F - L_F \tag{2.7}$$

where H_F is the height from the edge top of the inductor to the feed holder and L_F is the length of solid feed. The derivative gives

$$\frac{d}{dt}(h_F) = \frac{d}{dt}(H_F) - \frac{d}{dt}(L_F) \tag{2.8}$$

since the melting rate v_{Me} is defined as the change in the height of the upper zone and the pull rate of the feed v_F is defined as the change of the length of the solid feed, equation 2.8 can be written as the difference of the rate of melting and the feed pull rate.

$$\frac{d}{dt}(h_F) = v_{Me} - v_F \tag{2.9}$$

The same procedure can be done for the height of the lower zone, which gives

$$\frac{d}{dt}(h_C) = \frac{d}{dt}(H_c) - \frac{d}{dt}(L_C) = v_C - v_{Cr} \tag{2.10}$$

where h_C is the lower zone height, H_C is the length from the crystal holder to the edge of the inductor bottom, L_C is the length of the crystal. In a stationary case, the zone heights are constant, which implies the melting rate and the feed pull rate must be equal and that the crystallisation rate and the crystal pull rate must be equal too.

2.1.4 Volume of Visible Molten Material

The dynamics between the melt mass and the melt volume is described by the mass of the visible melt and the mass of the melt bowl hidden in the crystal. This equation is important for the mass balance in the process.

$$m_{melt} = m_{vi} + m_{bo} \tag{2.11}$$

The derivative of the melt mass is described as

$$\frac{d}{dt}(m_{melt}) = \frac{d}{dt}(m_{vi}) + \frac{d}{dt}(m_{bo}) \tag{2.12}$$

which can be rewritten as the incoming and outgoing melt flows

$$\frac{d}{dt}(m_{melt}) = -\dot{m}_F - \dot{m}_C \tag{2.13}$$

where the $\dot{m}_C$ is the change in the crystal mass due to crystallization and the m_F is the change in the feed crystal mass due to melting. The term $-m_F$ describes the flow of the melt mass from the feed crystal, which has to be negative due to that the mass of the feed crystal is reduced, in order to produce melt.
The derivative of the visible melt mass is described by equation 2.11 and 2.13

$$\frac{d}{dt}(m_{vi}) = -\dot{m}_F - \dot{m}_C - \frac{d}{dt}(m_{bo}) \tag{2.14}$$

The derivatives of the visible melt and the melt bowl can be written as

$$\begin{aligned} \rho_M \dot{V}_{vi} &= \frac{d}{dt}(m_{vi}) \\ \rho_M \dot{V}_{bo} &= \frac{d}{dt}(m_{bo}) \end{aligned} \tag{2.15}$$

where $\dot{V}_{vi}$ is the derivative of the visible melt volume, $\dot{V}_{bo}$ is the derivative of the melt bowl volume and ρ_M is the density of the melt.
The derivative $\dot{V}_{vi}$ considering equation 2.14 and 2.15 becomes

$$\rho_M \dot{V}_{vi} = -\dot{m}_F - \dot{m}_C - \rho_M \dot{V}_{bo} \tag{2.16}$$

The change of the solid feed mass above the line of melting can be calculated as the volume of a cone. See [1] appendix A.33. which leads to

$$\frac{d}{dt}(m_F) = \rho_S \pi R_F^2 \dot{L}_F + \dot{V}_{Fr} \tag{2.17}$$

where ρ_S is the density of the solid material, $\dot{V}_{Fr}$ is the change of the volume in the solid feed residual and R_F is the radius of the feed crystal at the line of melting. See figure 2.1. The complete derivative of the melt feed is described by equation 2.17 and 2.3

$$\dot{m}_F = \rho_S(\dot{V}_{Fr} - \pi R_F^2 v_{Me}) \tag{2.18}$$

The same substitutions can be done for the change in the crystal mass $\dot{m}_C$, which leads to the following equation

$$\dot{m}_C = \rho_S(\pi R_C^2 v_{Cr} - \dot{V}_{bo}) \tag{2.19}$$

Substituting equations 2.16, 2.18 and 2.19 the equation for $\dot{V}_{vi}$ is obtained. the parameters a_{Fr} and a_{bo} are introduced as fitting parameters to overcome errors in the approximation.

$$\rho_M \frac{d}{dt}(V_{vi}) = \rho_S(\pi R_f^2 v_{Me} - a_{Fr}\dot{V}_{Fr}) - \rho_S \pi R_C^2 v_{Cr} - (\rho_M - \rho_S) a_{bo} \dot{V}_{bo} \tag{2.20}$$

The stationary growth conditions, in which all derivatives are equal to zero, the following relation holds

$$R_F^2 v_F = R_C^2 v_C \tag{2.21}$$

which means that the stationary radius R_C can be calculated using only the feed pull rate v_F. the crystal pull rate v_C and the stationary feed radius R_C.

2.1.5 Volume of the Melt Bowl

The volume of the melt bowl V_{bo} is not directly measurable during an experiment, however in Werner [1] it was discovered that the behaviour of the bowl could be found to be an interpolating function depending on the crystal radius R_C. The equation is in the form

$$V_{bo} = \sum_{i=1}^{3} \left[a_i \left(R_C - a_0 \right) \right] \tag{2.22}$$

where a_i are model parameters used to fit the interpolation. The derivative of V_{bo} is

$$\dot{V}_{bo} = \dot{R}_C \sum_{i=1}^{3} \left[i \, a_i \left(R_C - a_0 \right)^{i-1} \right] \tag{2.23}$$

is applied in the melt volume equation in 2.1.4.

2.1.6 Solid Feed Residual Volume

The mass equation of the solid feed material consists of two parts, one part above the line of melting and one part below hidden by the melted material, which is called the solid feed residual. In Werner [1] the feed residual is described by a interpolating function of the feed rod radius

$$V_{Fr} = \sum_{i=1}^{3} d_i \left(R_F - d_0 \right)^i \tag{2.24}$$

The derivative of the residual V_{Fr} then depends of the feed radius and its derivative

$$\dot{V}_{Fr} = \dot{R}_F \sum_{i=1}^{3} i d_i (R_F - d_0)^{i-1} \tag{2.25}$$

is applied to the melt volume in section 2.1.4

2.1.7 Radius of the Melt Neck

The melt neck radius R_N was found experimentally to be a linear relationship with the full zone height h_G, however it is only linear if the crystal radius is larger than 20 mm [1]. The melt neck is considered negligible for crystal radius under 20 mm.

$$\frac{d}{dt}(R_N) = n_h(\dot{h}_F + \dot{h}_C) \tag{2.26}$$

where n_h is a model parameter, $\dot{h}_F$ is the derivative of the upper zone height and $\dot{h}_C$ is the derivative of the lower zone height.

2.1.8 Angle of the Crystal Rod

The angle of the crystal rod is found by solving the angle of the melt on the crystal rod. This is done by solving the Laplace-Young equation that describes the force equilibrium of a point on a melted drop. See Werner [1] and Coriell and Cordes [10] for a detailed analysis and explanation.

It is clear that the melt angle is dependent on the visible melt, the radius of the feed and crystal rods and the corresponding zone heights. However, for the cone, landing and growing phases, it is assumed the melt angle is dependent on the visible melt, the radius of the crystal rod and the corresponding zone height and the radius of the melt neck. The derivative becomes a partial differential equation which describes the dynamical behaviour of the melt angle. The variables $\dot{V}_{vi}$, $\dot{R}_C$, $\dot{h}_C$ and $\dot{R}_N$ are calculated by their respective differential equations 2.20, 2.6, 2.10 and 2.26.

The total differential equation for the melt angle becomes

$$\dot{\phi}_C = a_v \frac{\Delta\phi_M}{\Delta V_{vi}} \dot{V}_{vi} + a_r \frac{\Delta\phi_M}{\Delta R_C} \dot{R}_C + a_h \frac{\Delta\phi_M}{\Delta h_C} \dot{h}_C + a_N \frac{\Delta\phi_M}{\Delta R_N} \dot{R}_N \tag{2.27}$$

where the model parameter a_v, a_r, a_h, a_N are used to handle approximation errors. The difference quotients $\frac{\Delta\phi_M}{\Delta V_{vi}}$, $\frac{\Delta\phi_M}{\Delta R_C}$, $\frac{\Delta\phi_M}{\Delta h_C}$, $\frac{\Delta\phi_M}{\Delta R_N}$ are all assumed to depend on the crystal rod radius [1] and through experiments a look-up table was developed for each quotient, as seen in table 2.2. From the table 2.2 the signs of the quotients show: That a positive change in the melt volume will introduce a positive change in the crystal angle, a positive change in the lower zone height, crystal diameter or the melt neck will give a negative effect on the crystal angle.

R_C [mm]	$\Delta\phi_M/\Delta V_{vi}$ [$^\circ/\mathrm{cm}^3$]	$\Delta\phi_M/\Delta R_C$ [$^\circ$/mm]	$\Delta\phi_M/\Delta h_C$ [$^\circ$/mm]	$\Delta\phi_M/\Delta R_N$ [$^\circ$/mm]
10	72.27	-25.52	-23.65	-6.77
15	29.06	-20.47	-14.03	-3.91
20	15.45	-15.85	-8.56	-2.38
25	9.269	-12.34	-5.44	-1.59
30	6.22	-9.95	-3.83	-1.16
35	4.54	-8.69	-2.98	-0.87
40	3.43	-7.50	-2.33	-0.71
45	2.73	-6.81	-1.91	-0.55
50	2.15	-5.87	-1.60	-0.45
55	1.73	-4.99	-1.36	-0.34
60	1.43	-4.58	-0.87	-0.31
65	1.23	-4.31	-0.75	-0.27
70	1.06	-4.02	-0.71	-0.24

Table 2.2: Lookup table containing quotients for the crystal angle ϕ_C (From [1])

2.1.9 Inductor Coil Power

The power output of the conductor in the feed and crystal rods are given by a first order equation, as generator needs time to change the voltage output.

$$\frac{d}{dt}(P_{ind}) = \frac{1}{\tau_P}(K_P\, P_{gen} - P_{ind}) \tag{2.28}$$

which P_{ind} is the power output of the inductor going into the rods, τ_P is the time constant, K_P is a gain constant which is the amount of power lost between the generator power and the induced

power and P_{gen} is the power output of the generator. The power output of the generator cannot be directly adjusted on the FZ machines. Instead the equation 2.28 is converted to DC voltages. U_{gen} becomes the adjustable variable used to manipulate the heater power.

$$\dot{U}_{ind} = \frac{1}{\tau_P}(K_P U_{gen} - U_{ind}) \tag{2.29}$$

2.1.10 Rate of melting & Rate of crystallization

This describes the amount of heat energy required to change from solid to liquid $Q_{melting}$ or liquid to solid $Q_{crystalize}$

$$Q = q_0\, m \tag{2.30}$$

where q_0 is the latent heat coefficient of silicon, which is the specific energy needed to change a silicon mass from solid to a liquid or the opposite. The melting and crystallisation rates can be described by the required power to create a mass flow

$$\dot{m}_F = -\frac{P_{F,melting}}{q_0} \tag{2.31}$$

$$\dot{m}_C = -\frac{P_{F,Crystallize}}{q_0} \tag{2.32}$$

where $P_{F,melting}$ is the power used for melting, $P_{F,Crystalize}$ is the released power due to crystallization and. The energy in the rods is also lost due to radiation. The power term P_{loss} is approximated as a function of the radius of a rod.

$$P_{loss} = \zeta_{loss}\, R^{\frac{3}{2}} \tag{2.33}$$

These powers are used in a quasi-steady state balance equation for the feed and crystal rods.

$$0 = P_F - P_{F,loss} - P_{F,melting} \tag{2.34}$$

$$0 = P_C - P_{C,loss} + P_{C,crystalize} \tag{2.35}$$

where P_F and P_C is the induced in the feed and crystal rods, $P_{F,loss}$ and $P_{C,loss}$ is the power lost due to radiation, $P_{F,melting}$ is the power used in the melting process nad $P_{C,crystalize}$ is the power released due to crystallization. The variables P_F and P_C have been modelled using a heuristic approach in Werner [1]. The equations are modelled to reflect the following effects

- The induced power is increased if the power of the inductor increases.
- The induced power is increased if the radius if the corresponding rod increases.
- The induced power decreases if the corresponding zone height increases.

Using this approach the following equations was found to fulfil the requirements.

$$P_F = P_{ind,F} R_F^{r_F} (1 - f_0 h_F)^{f_1} \tag{2.36}$$

$$P_C = P_{ind,C} R_C^{r_C} (1 - c_0 h_C)^{c_1} \tag{2.37}$$

where P_{ind} is the amount of the inductor power that acts on the respective rods. The variables r_F, r_C, f_0, f_1, c_0 and c_1 are model parameters that is used to fit the equations with the experimental data found in Werner [1]. The terms $P_{ind,F}$ and $P_{ind,C}$ are adjusted by the generator voltage

$$P_{ind,F} = p_F U_{ind}^{e_F} \tag{2.38}$$

$$P_{ind,C} = p_C U_{ind}^{e_C} \tag{2.39}$$

where p_F, p_C, e_F and e_C are model parameters used to fit the equation with experimental data. The melting and crystallization rates can now be deducted. From equations 2.18, 2.31 and 2.34 a equation for the melting rate v_{Me} is found

$$v_{Me} = \frac{P_F - P_{F,loss}}{q_0 \rho_S \pi R_F^2} + \frac{\dot{V}_{Fr}}{\pi R_F^2} \tag{2.40}$$

and a equation for the crystallization rate can be found from equations 2.19, 2.35 and 2.32

$$v_{Cr} = \frac{P_{C,loss} - P_C}{q_0 \rho_S \pi R_C^2} + \frac{\dot{V}_{bo}}{\pi R_C^2} \tag{2.41}$$

and their respective derivatives are

$$\dot{v}_{Me} = \frac{1}{q_0 \rho_S \pi R_F^2} \left(\dot{P}_F - \dot{P}_{F,loss} - 2\frac{\dot{R}_F}{R_F} \left(P_F - P_{F,loss} \right) \right) + \frac{1}{\pi R_F^2} \left(\ddot{V}_{Fr} - 2\frac{\dot{R}_F}{R_F} \dot{V}_{Fr} \right) \tag{2.42}$$

$$\dot{v}_{Cr} = \frac{1}{q_0 \rho_S R_C^2} \left(\dot{P}_{C,loss} - \dot{P}_C - 2\frac{\dot{R}_C}{R_C} \left(P_{C,loss-P_C} \right) \right) + \frac{1}{\pi R_C^2} \left(\ddot{V}_{bo} - 2\frac{\dot{R}_C}{R_C} \dot{V}_{bo} \right) \tag{2.43}$$

CHAPTER 3

Model Analysis

In this chapter the linear model will be presented, which will form the basis for the controller and estimator design. The linear model will be represented in state space, as the non-linear equations are known and the conversion between ODE and state space is straight forward. The linear model will be found from a chosen operation point, from which an analysis of the stability of the linear model will be carried out.

3.1 Non-Linear Model

The non-linear model was presented in 2. The chosen states are show in the following non linear state space representation 3.1. The model contains nine ordinary differential equations where the state vector are $x = [R_F\ R_C\ h_F\ h_C\ \phi_C\ V_{vi}\ R_N\ U_{ind}\ v_{Me}\ v_{Cr}]$, with the input variables $u = \begin{bmatrix} U_{gen} & v_F & v_C \end{bmatrix}$ and the disturbance $d = \begin{bmatrix} \alpha_F \end{bmatrix}$.

$$\begin{bmatrix} \dot{R}_F \\ \dot{R}_C \\ \dot{h}_F \\ \dot{h}_C \\ \dot{\phi}_C \\ \dot{V}_{vi} \\ \dot{R}_N \\ \dot{U}_{ind} \\ \dot{v}_{Me} \\ \dot{v}_{Cr} \end{bmatrix} = \begin{bmatrix} v_{Me}\tan(\alpha_F) \\ v_{Cr}\tan(\phi_C) \\ v_{Me} - v_F \\ v_C - v_{Cr} \\ a_v\frac{\Delta\phi_M}{\Delta V_{vi}}\dot{V}_{vi} + a_r\frac{\Delta\phi_M}{\Delta R_C}\dot{R}_C + a_h\frac{\Delta\phi_M}{\Delta h_C}\dot{h}_C + a_N\frac{\Delta\phi_M}{\Delta R_N}\dot{R}_N \\ \rho_S(\pi R_f^2 v_{Me} - a_{Fr}\dot{V}_{Fr}) - \rho_S\pi R_C^2 v_{Cr} - (\rho_M - \rho_S)a_{bo}\dot{V}_{bo} \\ n_h(\dot{h}_F + \dot{h}_C) \\ \frac{1}{\tau_P}(K_P U_{gen} - U_{ind}) \\ \frac{1}{q_0\rho_S\pi R_F^2}\left(\dot{P}_F - \dot{P}_{F,loss} - 2\frac{\dot{R}_F}{R_F}(P_F - P_{F,loss})\right) + \frac{1}{\pi R_F^2}\left(\ddot{V}_{Fr} - 2\frac{\dot{R}_F}{R_F}\dot{V}_{Fr}\right) \\ \frac{1}{q_0\rho_S R_C^2}\left(\dot{P}_{C,loss} - \dot{P}_C - 2\frac{\dot{R}_C}{R_C}(P_{C,loss-P_C})\right) + \frac{1}{\pi R_C^2}\left(\ddot{V}_{bo} - 2\frac{\dot{R}_C}{R_C}\dot{V}_{bo}\right) \end{bmatrix} \tag{3.1}$$

3.1.1 Operation Point

The operation point for this analysis has been chosen to be at the point where the crystal diameter is 6 inches (152.4 mm) and assumed that this point is stationary. The initial values for the states are determined from measurements of a production run[1]. The operation point in the dataset are not equilibrium points, due to offsets in the measurement and estimation, however, these values can be used as an initial point for the stationary calculation. First the assumption must be made that the process in this point is at an equilibrium, which means that all the derivatives must be equal to zero, the generator voltage must be equal to the inductor voltage of the system $U_{gen} = U_{ind}$ and that the feed rod angle α_F and the crystal angle ϕ_C are equal to zero. The feed pull rate must be equal to the melting rate $v_F = v_{Me}$ and the crystal pull rate must be equal to the crystallisation rate $v_C = v_{Cr}$. Remembering equation 2.21, which tells that a stationary growth can be found when the two sides are equal. Using these assumptions and the equation 2.21 a stationary point x_{ss} can be calculated.

The operation point values x_e and the steady state values x_{ss} are shown in table 3.1. Note that the crystal angle ϕ_C and the crystallization rate v_{Cr} have been adjusted to fit stationary growth conditions.

	R_F	R_C	h_F	h_C	ϕ_C	V_{vi}	R_N	U_{ind}	v_{Me}	v_{Cr}
	$[mm]$	$[mm]$	$[mm]$	$[mm]$	$[^\circ]$	$\left[cm^3\right]$	$[mm]$	$[kV]$	$\left[\frac{mm}{min}\right]$	$\left[\frac{mm}{min}\right]$
x_e	170.04	152.40	5.379	9.361	0.08	152.787	10.195	7.856	2.014	2.46
x_{ss}	170.04	152.40	5.379	9.361	0	152.787	10.195	7.856	2.014	2.510

Table 3.1: Table of state variables of chosen operation point x_e and the adjusted steady state point x_{ss}

3.1.2 Step Response of The Non-Linear Model

In this section the step responses of the non-linear model are evaluated. This is a important step in understanding the dynamic behaviour of the model. Figure 3.1 shows the response of the crystal diameter D_C, as this is the most important variable, in three simulations a, b and c and figure 3.2 shows in corresponding inputs. Each simulation has a duration of 30 minutes, a change in the inputs is carried out in the time interval $3\,\mathrm{min} \leq t \leq 30\,\mathrm{min}$, with a step size of 1% of the inputs steady state values.

In (a) the feed and crystal pull rates are kept constant at the equilibrium point and the generator voltage U_{gen} is increased by 1% after 3 minutes. This increases the induced power in both the feed and crystal rods. The dynamic behaviour of the crystal diameter have three phases.

[1]These datasets are confidential and have been provided by Topsil GlobalWafers A/S.

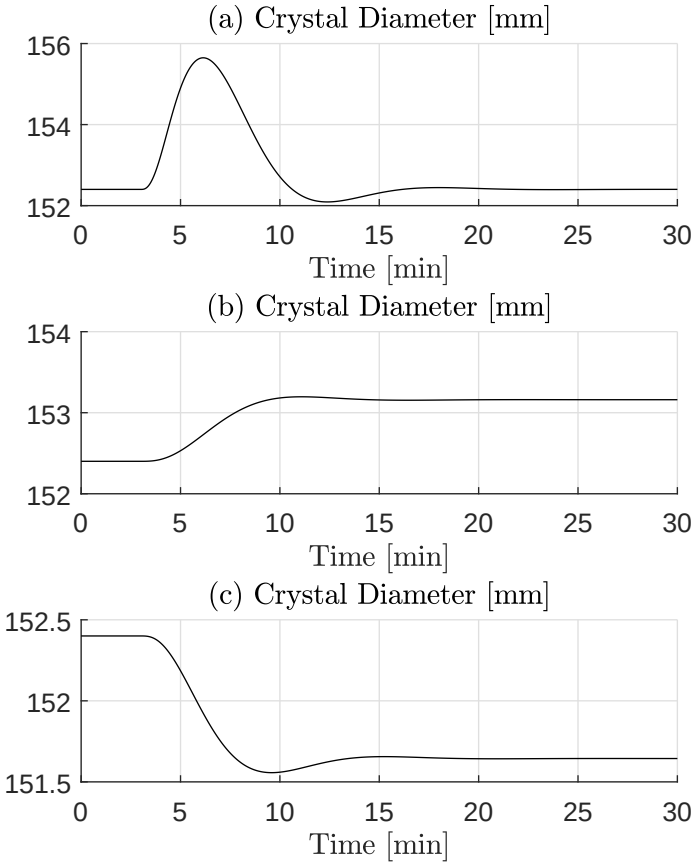

Figure 3.1: Step Response - State variables

In the first phase, the diameter starts increasing when the change is introduced. This due to an acceleration in the induced power, which increases the melting rate and moves the melting line further away from the inductor, increasing the upper zone height. The crystallisation rate of the crystal rod decreases due to extra energy from the inductor, which moves the crystallisation line further away from the inductor. This increases the volume of the melt and also creates a melt overhang that increases the angle of the crystal rod and the crystal diameter grows.

After about 6 minutes the crystal diameter starts decreasing, which is the second phase of the response. The second phase is due to the deceleration in the induced power as it settles at its new value. The crystallisation rate now begins to increase and the melting rate begins to decrease, this causes a decrease in the volume of the melt. The crystal angle in decreased due to the melt overhang disappearing and the crystal diameter begins to shrink.

In the third phase, after about 20 minutes, of the response, the process has begun to settle. The melting and crystallisation rate, the crystal diameter, melt volume and crystal angle settles at the original steady state values. This is because of the mass balance since there is no extra material introduced into the system, which can only be done by increasing the feed pull rate, which can be seen in figure 3.1 (b). The full state response for simulation (a) can be seen in appendix 7.2 in figure 1.

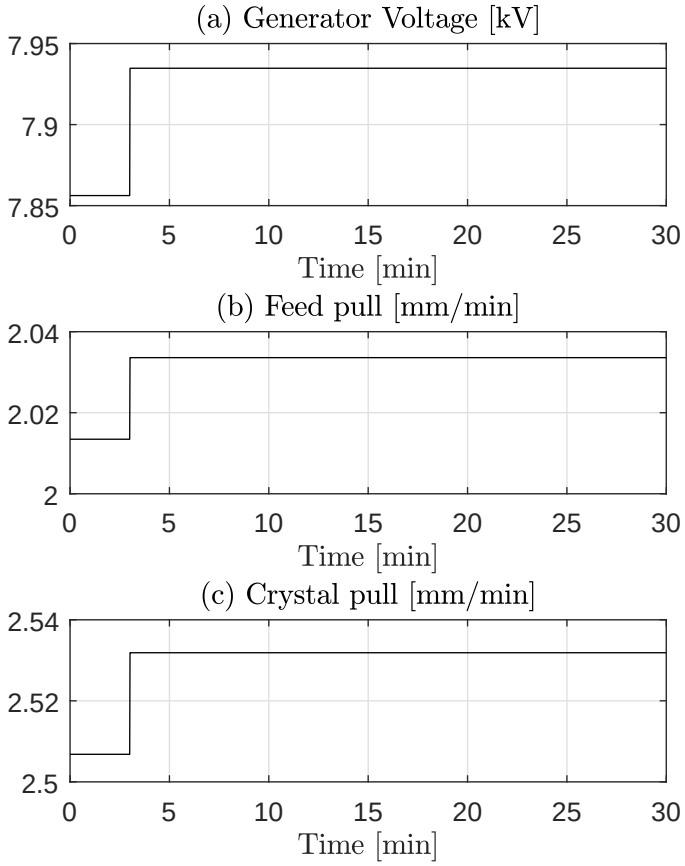

Figure 3.2: Step Response - Input Variables

In figure 3.1(b) the generator voltage U_{gen} and crystal pull rate v_C are kept constant. The feed pull rate v_F is increased by 1% of the steady state value. In other words, the feed rod is pushed faster downwards, increasing the amount of material that is put into the process.

The response in (b) in intuitively easier to follow. The increased feed pull rate decreases the upper zone height, moving the melting line closer to the inductor, which increases the melting rate. The increased melting rate increases the amount of melt in the process, which increases the crystal angle due to the appearance of a melt overhang. This increases the crystal diameter. The crystal diameter settles to a new equilibrium in about 12 minutes because the melting rate settles. The process will be at an equilibrium point if the inductor power, crystallisation and melting rates are constant.

The full state response for simulation (b) is located in appendix 7.2 in figure 2.

In figure 3.1(c) the inductor and feed pull rate are kept constant. The crystal pull rate is increased by 1% of the steady state This causes the crystal rod to be pulled faster downwards away from the inductor. This action increases the crystallisation rate because the amount of power induced in the crystal rod decreases. The crystal diameter decreases because the amount of melt on the crystal rod decreases and the increase in the lower zone height.

To summarise the crystal diameter can only be increased or decreased permanently by manipulating either the feed pull rate v_F or the crystal pull rate v_C as seen in 3.1(b) and (c) respectively. The inductor power U_{gen} can be used to improve the transients that occur when manipulating the pull rates, which is a behaviour that will be used in the control design.

3.2 Linear Model

The non-linear state space model is to be linearised, such that the dynamic and transient behaviour can be approximated and the system can be represented by state space. The non-linear model is linearised around the equilibrium point x_{ss} with a Jacobian linearisation. The linearisation will produce a linear time invariant model that is based on deviations from the linearised point.

State Space Representation

The continuous time invariant state space formulation is given as

$$\begin{aligned} \dot{x}(t) &= \mathbf{A}x(t) + \mathbf{B}u(t) + \mathbf{E_d}d(t) \\ y(t) &= \mathbf{C}x(t) \end{aligned} \tag{3.2}$$

where $\mathbf{A}$ is the state dynamics matrix, with the state vector $x(t) = [R_C\, h_F\, h_C\, \phi_C\, V_{vi}\, R_N\, U_{ind}\, v_{Me}\, v_{Cr}]$, the input dynamics matrix $\mathbf{B}$ with the input vector $u(t) = \begin{bmatrix} U_{gen} & v_F & v_C \end{bmatrix}$. The output dynamics matrix $\mathbf{C}$. $\mathbf{E}_d$ is the unknown disturbance dynamics matrix, with the disturbance vector $d(t)$. The system matrices are found by Jacobian linearisation of the non-linear model as described in [11].

The continuous model 3.2 have been discretized assuming a zero-order hold, with regards a chosen sample time and is given by

$$\begin{aligned} x_{k+1} &= \mathbf{F}x_k + \mathbf{G}u_k \\ y_k &= \mathbf{C}x_k \end{aligned} \tag{3.3}$$

where $\mathbf{F}$ is the discrete state dynamics matrix, $\mathbf{G}$ is the discrete input dynamics matrix, $\mathbf{G}_d$ and x_k, u_k and d_k are the discrete state, input and disturbance vectors in discrete time. The discrete model will be used for the design of the model predictive controller.

3.3 Stability Analysis

A stability analysis aims to give an answer to if the process has a stable or unstable response, where an unstable response is almost always an unwanted behaviour in the system, but it can be made stable under the right conditions which will be discussed in 3.5. The stability of this process will be determined by an analysis of the eigenvalues. Eigenvalues and eigenvectors are an important tool

for the stability analysis and the dynamic responses of linear models. In short the eigenvalues of the state dynamics matrix are the poles of the system and are often used in when analysing multiple input multiple output systems (MIMO) [11].

To be able to define the stability of the process, an equilibrium point must be defined. A point x_e is an equilibrium point for the process if the process starts or remains at this point in the absence of inputs and disturbances. An equilibrium point can be defined as a stationary state point (see [11, page 119]).
A unique equilibrium point is found if $\mathbf{A}$ is non-singular. A matrix is singular if and only if the determinant is equal to zero.

Location of eigenvalues

The eigenvalues λ of the linear model are found by calculating the characteristic polynomial of the state matrix $\mathbf{A}$. The stability of the process is determined by the location of the eigenvalues. It is stated in [12, page 24-33] that the system is asymptomatically stable if all the negative and negative complex eigenvalues will be stable and the response will be oscillating. If any of the eigenvalues are positive, then the system response is unstable. A special case is when one or more of the eigenvalues are zero, the system can then be stable or unstable in any equilibrium point and there are infinite equilibrium points.
The calculated eigenvalues of the linear model linearized around the operating point are

$$\lambda = \begin{bmatrix} 0 \\ 0 \\ 0 \\ -0.005 + 0.009i \\ -0.005 - 0.009i \\ -0.022 \\ 0 \\ -0.009 \\ -0.050 \end{bmatrix} \tag{3.4}$$

which shows that the system is stable, as there are no positive eigenvalues. The response of the system will also show some oscillating behaviour because of the complex eigenvalue pair $-0.005 \pm +0.009i$. However there are also multiple zero eigenvalues; which means that the system is not asymptotically stable since the system is only stable if all eigenvalues have a non-zero negative real part, however it could be marginally stable. The system is marginally stable if zero eigenvalues are simple. Since the zero eigenvalues are repeated they are not simple. However the system can also be marginally stable if the eigenvectors V_λ associated with the zero eigenvalues are linearly independent.

The eigenvectors to the zero eigenvalues are

$$V_{\lambda=1,2,3,7} = \begin{bmatrix} 0 & 0 & 0 & 0 \\ 0 & 0 & 0 & 1 \\ 1 & 0 & 0 & 0 \\ 0 & 0 & 0 & 0 \\ 0 & 1 & 0 & 0 \\ 0 & 0 & 1 & 0 \\ 0 & 0 & 0 & 0 \\ 0 & 0 & 0 & 0 \\ 0 & 0 & 0 & 0 \end{bmatrix} \tag{3.5}$$

which shows that the eigenvectors are linearly independent of each other. The system can be called marginally stable, which also shows in the system response, the process will stabilize at a new equilibrium if perturbations happens on the zero eigenvalues. It also means that the system is stable around a equilibrium subspace, which can hold infinite equilibrium points.

3.4 Linear Response

In this section the linear model is tested against the non-linear model, to verify that it can accurately depict the response of the non-linear system. It should be noted as stated in section 3.2 that by the definition of the linearisation, the linear model is only accurate within a small deviation from the operation point. The numerical accuracy of the linear model will be evaluated by the mean square error. The MSE calculates the average value of the residuals, the differences between two models, which always have a positive value. The closer the MSE is to zero, the better the depiction is, which in this case is the linear model. The equation for the MSE is

$$\text{MSE} = \frac{\|y_{linear} - y_{nonlinear}\|^2}{N} \tag{3.6}$$

where y_{linear} is the output of the linear model, $y_{nonlinear}$ is the output of the non-linear value and N is the number of samples in the outputs. The MSE method is, however, sensitive to large residuals as it weighs those more heavily than small residuals, however since the simulations are deterministic in nature, there will not be relatively large residuals, as these most often occur when noise is present. Another method could have been the mean absolute error.
Figure 3.3 shows three simulations of the crystal diameter. For each simulation the inductor power is increased by 1%(3.3(a, black)), 5%(3.3(b, blue)) and 9%(3.3(c, red)). and the respective of the non-linear model and the linear model.

Figure 3.4 shows the respective step changes corresponding to the three simulations. In Figure 3.3 the non-linear model shows that the crystal diameter peaks at about 156 mm, and the linear model follows the same dynamic and the MSE value is close to zero 3.2. This means that the linear model can accurately calculate the non-linear model within a 1% change in the inductor power. However in figure 3.3 (b) there is clearly a difference in the dynamic responses of the two models and the

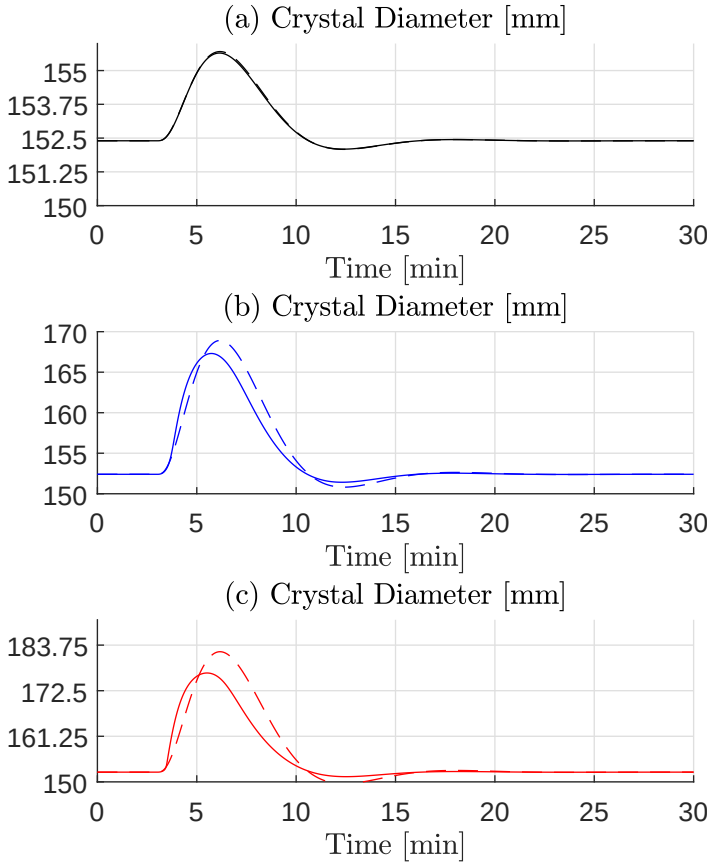

Figure 3.3: Comparison of the non-linear model (full line) and the linear model (stripped line) with different increases in inductor power: 1% black line (a), 2% blue line (b) and 9% red line (c).

MSE value has increased. In figure 3.3 (c) there a large deviation between the two models and there is even a difference in the dynamic behaviour as seen at time 4 min. The MSE is significantly larger.

MSE	1%	5%	9%
R_C	1×10^{-4}	0.2739	2.2217

Table 3.2: The MSE value for the crystal diameter R_C. Each column represents the step size in the inductor voltage U_{gen}
,

This behaviour means that when the linear model becomes increasingly unable to calculate the non-linear model, if the inputs are changed from the steady state value. A change between 1% to 5% gives a fairly accurate depiction, however a larger step would increase the non-linearities behaviour which the linear model is not able to calculate.

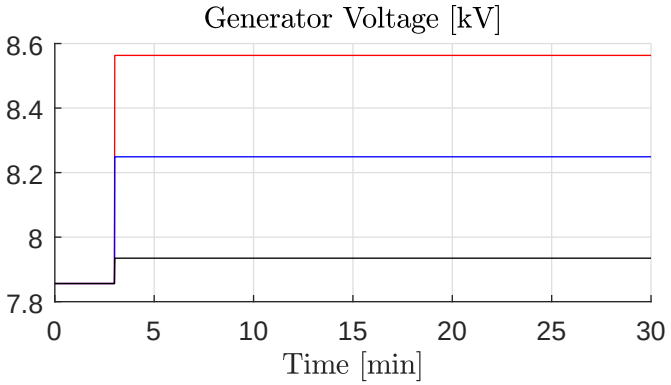

Figure 3.4: Black line: 1% step change of steady state value. Blue Line: 5% step change of steady state value. Red Line: 9% step change of steady state value

3.5 State Space Analysis

Controllability and Observability

Before designing a control system, several properties of the linear model has to be investigated, namely controllability and observability, and the sub-properties stabilizability and detectability. Many of the controller design methods depends on this properties to be fulfilled.

3.5.1 Reachability

Reachability gives an answer to the question: is there a sequence of control inputs which will bring the initial state to any final state. The fastest way to ensure that the system is fully reachable is to check if the reachability matrix **M** has full rank. A matrix has a full rank when the number of linearly independent columns is equal to the number of rows. The reachability matrix number of rows equal the number of states in the system matrix. The reachability matrix is often called the controllability matrix, as it is the same calculation done in continuous time [11] and it is described as

$$\mathbf{M} = \begin{bmatrix} \mathbf{G} & \mathbf{FG} & \mathbf{F}^2\mathbf{G} & \dots & \mathbf{F}^{n-1}\mathbf{G} \end{bmatrix} \tag{3.7}$$

where $\mathbf{F}$ is the state matrix, $\mathbf{G}$ is the input matrix and n is the number of states. The rank of reachability matrix M is found to be

$$\text{rank}(M) = 5 \tag{3.8}$$

The reachability matrix has only 5 linear independent column, which by the definition in [11, page 140], since it should have a rank of 9, which makes it not fully reachable, or fully controllable.

3.5.2 Stabilizability

Since the system is not fully reachable, it has to be investigated if it is stabilizable. A system is stabilizable if the unstable eigenvalues are in the controllable subspace, in other words, the controller is able to stabilise the unstable behaviour and if the uncontrollable eigenvalues are stable [11]. This done by using the first decomposition Theorem in [11, page 154]. First, the system is decomposed into a controllable and uncontrollable subspace to investigate the uncontrollable properties of the system. A similarity transformation from $x\ to\ \bar{x}$ is used with the transformation matrix V.

$$\bar{x} = \mathbf{V}^{-1}x \tag{3.9}$$

such that the transformed system has the same structure and dynamic response of the original system. The state vector will be composed of the controllable $\bar{x}_c$ and uncontrollable $\bar{x}_{uc}$ eigenvalues.

$$\begin{aligned} \begin{bmatrix} \bar{x_c} \\ \bar{x}_{uc} \end{bmatrix}_{k+1} &= \bar{\mathbf{F}}\bar{x} + \bar{\mathbf{G}}u \\ y &= \bar{\mathbf{C}}\bar{x} \end{aligned} \tag{3.10}$$

where the state dynamics matrix $\bar{\mathbf{F}}$ is now given as

$$\bar{\mathbf{F}} = \mathbf{V}^{-1}\mathbf{A}\mathbf{V} = \begin{bmatrix} \bar{\mathbf{F}}_{11} & \bar{\mathbf{F}}_{21} \\ 0 & \bar{\mathbf{F}}_{22} \end{bmatrix} \tag{3.11}$$

and the input dynamics $\bar{\mathbf{G}}$ and the output dynamic $\bar{\mathbf{C}}$ matrices are given as

$$\bar{\mathbf{G}} = \mathbf{V}^{-1}\mathbf{A} = \begin{bmatrix} \bar{\mathbf{G}}_1 \\ 0 \end{bmatrix} \tag{3.12}$$

$$\bar{\mathbf{C}} = \mathbf{C}\mathbf{V} = \begin{bmatrix} \bar{\mathbf{C}}_1 & \bar{\mathbf{C}}_2 \end{bmatrix} \tag{3.13}$$

Where the controllable subspace is given by

$$\begin{aligned} \bar{x}_{c,k+1} &= \bar{\mathbf{F}}_{11}\bar{x}_{c,k} + \mathbf{G}_1 u_k \\ y_k &= \bar{\mathbf{C}}_1\bar{x}_{c,k} \end{aligned} \tag{3.14}$$

and the uncontrollable subspace in discrete time is given by

$$\begin{aligned} \bar{x}_{uc,k+1} &= \bar{\mathbf{F}}_{22}\bar{x}_{uc,k} + \mathbf{0}u_k \\ y_k &= \bar{\mathbf{C}}_2\bar{x}_{uc,k} \end{aligned} \tag{3.15}$$

and the uncontrollable subspace in continous time can be given by the same structure

$$\begin{aligned} \dot{\bar{x}}_{uc,t} &= \bar{\mathbf{A}}_{22}\bar{x}_{uc,t} + \mathbf{0}u_t \\ y_t &= \bar{\mathbf{C}}_2\bar{x}_{uc,t} \end{aligned} \tag{3.16}$$

The eigenvalues of the continuous time uncontrollable subspace matrix $\bar{A}_{22}$ are

$$\lambda_{22} = \begin{bmatrix} -6.6243 \times 10^{-6} \\ 0 \\ 0 \\ 0 \end{bmatrix} \tag{3.17}$$

The uncontrollable eigenvalues are marginally stable which means the system is stabilizable.

3.5.3 Observability

Observability gives an answer to the question: Is it possible to determine the value of all the states given the knowledge available in the system output. Again the procedure to find the observability matrix is to use the observability matrix $\mathbf{O}$ and check if this has full rank. The observability matrix is given by

$$\mathbf{O} = \begin{bmatrix} \mathbf{C} & \mathbf{CA} & \mathbf{CA}^2 & ... & \mathbf{CA}^{n-1} \end{bmatrix}^T \tag{3.18}$$

where $\mathbf{A}$ is the state matrix, C is the output dynamics matrix and n is the number of rows is F. The rank controllability matrix $\mathbf{O}$ is found to be

$$\text{rank}(O) = 9 \tag{3.19}$$

The observability of this system is found to be fully observable. Which in practice means that each state can be observed by the controller. If the system was found to be not fully observable the control designer would have to design an observer.

CHAPTER 4

Control Theory

4.1 Model Predictive Controller

The chosen controller for this system is the model predictive controller. This controller is an optimal controller that solves a given optimisation problem, such as minimization or maximisation of a cost function. Usually minimization of the error between the output measurement and the reference. It uses a prediction horizon to calculate the optimal control signal, with the advantage of solving the problem considering system constraints. This gives the advantage to using the controller for sensitive systems, where the plant needs to be operated near the boundaries and systems with careful safety constraints.

In this thesis, a model predictive controller is chosen with is a quadratic cost function and is using a moving prediction horizon. A moving horizon implementation means that the optimisation calculations are updated each time there is new information in the form of new measurements. The MPC calculates the optimal input sequence for the length of the prediction horizon, however only the first value in the sequence is used, such that the output is regulated. This approach is called the moving horizon control. An additional application is that the output of the plant needs to track a given reference or there is a disturbance that needs to be rejected.

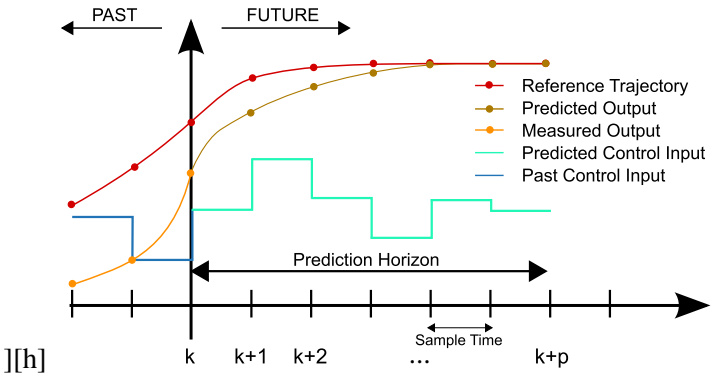

Figure 4.1: A sketch of the measured, predicted, and input variables in a model predictive control scheme. (By Martin Behrendt - CC BY-SA 3.0, https://commons.wikimedia.org/w/index.php?curid=7963069)

A moving prediction horizon as seen in figure 4.1 uses a window with a finite number of samples, from sample k to $k + Np$ (the horizon, blue line) to predict the future output of the plant (the dotted brown line), and at each new time sample the window is moved [13] [14] [2] . The longer the horizon is chosen to be the better steady state performance the controller is going to have, however, the computation time also increases, which means that if the sampling time of the controller is shorter than the computation time, the online computation approach will be impossible.

4.1.1 Unconstrained MPC Design

The basic formulation of the MPC is the unconstrained case, where no boundary conditions are taken into account. The most common formulation is where the optimization variable is a control move δu instead of the normal control signal of u_k [13]. The objective function is chosen to be a minimization of the controlled output z_k and reference r_k error vector. A weighted 2-norm is used when solving the least square problem. The dynamic quadratic program becomes

$$\begin{aligned} \min_{U} \quad & \phi_z = \frac{1}{2}\sum_{k=0}^{N} \|z_k - r_k\|^2_{W_z} \\ \text{s.t.} \quad & x_{k+1} = \mathbf{F}x_k + \mathbf{G}u_k \\ & z_k = \mathbf{C}_z x_k \qquad\qquad k = 0, 1, ..., N-1 \\ & y_k = \mathbf{C}_y x_k \qquad\qquad k = 0, 1, ..., N-1 \end{aligned} \tag{4.1}$$

where the error vector is weighted with W_z and the prediction horizon is written as N_p. Both the prediction horizon and the weight W_z are the tuning parameters for this controller. The cost function in 4.1 can be expressed in standard QP problem notation with the following vector notation, called the weighted least squares problem

$$\min \phi = \frac{1}{2}x'Hx + gx + p \tag{4.2}$$

$$\begin{aligned} U^* = \min \quad & \phi = \frac{1}{2}\sum_{k=1}^{N} \|\mathbf{\Gamma}U - \mathbf{b}\|^2_{W_z} \\ & b = R - \mathbf{\Phi}x_k \end{aligned} \tag{4.3}$$

which is a compact form of the system matrices based on the system's controlled outputs. The recursive formulation in 4.4 bring the formulation to the form in 4.2 since most QP solver use this notation

$$\begin{aligned} \phi \quad =& \frac{1}{2}\sum_{k=1}^{N} \|\mathbf{\Gamma}U - \mathbf{b}\|^2_{W_z} \\ =& \frac{1}{2}(\Gamma U - b)'W_z(\Gamma U - b) \\ =& \frac{1}{2}U'\Gamma'W_z\Gamma U - (\Gamma'W_z b)'U + \frac{1}{2}b'W_z b \\ =& \frac{1}{2}U'HU + g'U + p \end{aligned} \tag{4.4}$$

where the matrices H, g and p described as

$$H = U'\Gamma'W_z\Gamma U = \Gamma'_U W_z \Gamma_U \tag{4.5}$$

$$\begin{aligned} g &= -(\Gamma' W_z b)' U = -\Gamma_U' W_z b \\ &= -\Gamma_U' W_z (R - \Phi x_k) \\ &= \Gamma_U W_z \Phi x_k - \Gamma_U W_z R \end{aligned} \tag{4.6}$$

The control law of the controller becomes

$$U^* = -H^{-1} \cdot g \tag{4.7}$$

where the hessian matrix H and the linear coefficient vector g expresses the internal gains of the controller.

$$\begin{aligned} M_x &= \Gamma_U W_z \Phi \\ M_r &= \Gamma_U W_z \\ g &= M_x x + M_r R \end{aligned} \tag{4.8}$$

The parameters Φ, Γ and b are found from the output prediction equation Z

$$\mathbf{Z} = \mathbf{\Phi} x_k + \mathbf{\Gamma} U + \mathbf{\Gamma}_D D \tag{4.9}$$

where the parameters Γ_u, Γ_d and Φ hold the information of systems behaviour for the prediction horizon.

$$R = \begin{bmatrix} r_1 \\ r_2 \\ \vdots \\ r_{Np} \end{bmatrix} \quad Z = \begin{bmatrix} z_1 \\ z_2 \\ \vdots \\ z_{N_p} \end{bmatrix} \quad U = \begin{bmatrix} u_0 \\ u_1 \\ \vdots \\ u_{N_p-1} \end{bmatrix} \quad D = \begin{bmatrix} d_1 \\ d_2 \\ \vdots \\ d_{(Np-1)} \end{bmatrix} \tag{4.10}$$

$$\bar{\mathbf{W}}_z = \begin{bmatrix} \mathbf{W}_{z,1} & 0 & 0 & 0 \\ 0 & \mathbf{W}_{z,2} & 0 & 0 \\ \vdots & \vdots & \ddots & \vdots \\ 0 & 0 & 0 & \mathbf{W}_{z,Np} \end{bmatrix} \tag{4.11}$$

where $r_{N_p} \in \Re^{n_z}$ is the vector for the reference values, $z_{N_p} \in \Re^{n_z}$ is the vector for the controlled output predictions, U is the vector of predicted inputs, and D is the vector of predicted disturbances. The expanded weighting matrix $\bar{W}_z$ is the a diagonal matrix containing the output weight matrix W_z for each time sample in the prediction horizon. The parameters ϕ, Γ_u and Γ_D are expressed as

$$\mathbf{\Phi} = \begin{bmatrix} \mathbf{C}_z \mathbf{A} \\ \mathbf{C}_z \mathbf{A}^2 \\ \mathbf{C}_z \mathbf{A}^3 \\ \vdots \\ \mathbf{C}_z \mathbf{A}^{N_p} \end{bmatrix} \tag{4.12}$$

$$\mathbf{\Gamma}_U = \begin{bmatrix} \mathbf{H}_{1,u} & 0 & 0 & \cdots & 0 \\ \mathbf{H}_{2,u} & \mathbf{H}_{1,u} & 0 & \cdots & 0 \\ \mathbf{H}_{3,u} & \mathbf{H}_{2,u} & \mathbf{H}_{1,u} & \cdots & 0 \\ \vdots & \vdots & \vdots & \ddots & \vdots \\ \mathbf{H}_{N_p,u} & \mathbf{H}_{N_p-1,u} & \mathbf{H}_{N_p-2,u} & \cdots & \mathbf{H}_{1,u} \end{bmatrix} \tag{4.13}$$

where $\mathbf{H}_u$ is the impulse response coefficients of the system with respect to input matrix.

$$\mathbf{H}_{i,u} = \mathbf{C}_z \mathbf{A}^{i-1} \mathbf{B} \tag{4.14}$$

To summarise the QP formulation, which is solved with the MATLAB function *quadproc*, for the unconstrained model predictive controller becomes

$$\begin{aligned} \underset{U}{min} &= \frac{1}{2} U' H U + g' U \\ H &= \Gamma_U' W_z \Gamma_U \\ g &= M_x x_k + M_r R \end{aligned} \tag{4.15}$$

Unconstrained MPC with Weighed Rate of Movement

A regularized therm $\phi_{\Delta u}$ is added to the problem, such that input can be weighted. In a LQR formulation it is the absolute value of the control signal u_k that is weighted, however since this signal can change erratic regardless of the weight, the control move $\Delta u_k$is considered instead. This will allow the controller to produce a smooth output. It should be noted that the same effect can be produced by having the control signal u_k run at the rate of input constraint, however this is not practical as the constraints are recommend for limitations in the process and actuators and not for controller tuning.
The following cost function is added to the original cost function in equation 4.1.

$$\min_U \phi_{\Delta u} = \frac{1}{2} \sum_{k=0}^{N-1} \|\Delta u_k\|^2_{W_u} \tag{4.16}$$

such that the complete cost function becomes

$$\min_U \phi = \frac{1}{2} \sum_{k=1}^{N} \|z - r\|^2_{W_z} + \frac{1}{2} \sum_{k=0}^{N-1} \|\Delta u_k\|^2_{W_u} \tag{4.17}$$

The new cost function in equation 4.16 can be written as

$$\begin{aligned} \|\Delta u_k\|^2_{W_{\Delta u}} &= \|u_k - u_{k-1}\|^2_{W_{\Delta u}} \\ \phi_{\Delta u} &= \frac{1}{2} U' H_{\Delta u} U + g'_{\Delta u} U \end{aligned} \tag{4.18}$$

where the hessian $H_{\Delta u}$ and $g_{\Delta u}$ are given by

$$H_{\Delta u} = \begin{bmatrix} 2W_{\Delta u} & -W_{\Delta u} & & \\ -W_{\Delta u} & 2W_{\Delta u} & -W_{\Delta u} & \\ & -W_{\Delta u} & 2W_{\Delta u} & -W_{\Delta u} \\ & & -W_{\Delta u} & W_{\Delta u} \end{bmatrix} \tag{4.19}$$

$$g_{\Delta u} = - \begin{bmatrix} W_{\Delta u} \\ 0 \\ \vdots \\ 0_{N_p} \end{bmatrix} \tag{4.20}$$

The complete quadratic program becomes:

$$\begin{aligned} \min_U &= \frac{1}{2}U'HU + g'U \\ H &= \Gamma_U' W_z \Gamma_U + H_{\Delta u} \\ g &= g + g_{\Delta u} \\ &= M_x x_k + M_r R + M_{u-1} \end{aligned} \tag{4.21}$$

It is to be noted that the gain matrices M_x, M_r and M_{u-1} does not change with time, they are time invariant which means that they can be calculated offline during the design phase of the controller, however the matrix g and H change at each time step, as the states and references change and they have to be calculated online.

4.1.2 Input rate constrained MPC

As the states earlier the nature of the MPC is that it can handle constraints naturally, since using quadratic programming allows the use of constraints to solve the system with linear inequalities, linear equalities and upper and lower bounds. Here the input rate constraint will be presented as a linear inequality, as the equipment in practise are bounded by rate limits. The objective function of the controller with the linear inequalities becomes

$$\min_U \phi = \phi_z + \phi_{\Delta u} = \frac{1}{2}\sum_{k=1}^{N} \|z_k - r_k\|^2_{W_z} + \frac{1}{2}\sum_{k=0}^{N-1} \|\Delta u_k\|^2_{W_u} \tag{4.22}$$

$$\begin{aligned} &\text{s.t.} \\ x_{k+1} \quad &= \mathbf{F}x_k + \mathbf{G}u_k \\ z_k \quad &= \mathbf{C}_z x_k \qquad\qquad k = 0, 1, ..., N-1 \\ y_k \quad &= \mathbf{C}_y x_k \qquad\qquad k = 0, 1, ..., N-1 \\ \Delta u_{min} \quad &\leq \Delta u_k \leq \Delta u_{max} \quad k = 0, 1, ..., N-1 \end{aligned} \tag{4.23}$$

This enables the specification of minimum and maximum rates of change of the control move. The constraint was implemented in the following way such that it can be used in the quadratic programmer.

$$\begin{bmatrix} \Delta U_{min} \\ \Delta U_{min} \\ \vdots \\ \Delta U_{min} \end{bmatrix} \leq \begin{bmatrix} -I & I & 0 & ... & 0 \\ 0 & -I & I & \ddots & \vdots \\ \vdots & \ddots & \ddots & \ddots & 0 \\ 0 & ... & 0 & -I & I \end{bmatrix} \begin{bmatrix} U_1 \\ U_2 \\ \vdots \\ U_{N-1} \end{bmatrix} \leq \begin{bmatrix} \Delta U_{max} \\ \Delta U_{max} \\ \vdots \\ \Delta U_{max} \end{bmatrix} \tag{4.24}$$

The quadratic program now can be formulated as

$$\begin{aligned} \min_{U} &= \frac{1}{2}U'HU + g'U \\ H &= \Gamma'_U W_z \Gamma_U + H_{\Delta u} \\ g &= g + g_{\Delta u} \\ &= M_x x_k + M_r R + M_{u-1} \\ &s.t. \\ &\Delta u_{min} \leq \Delta u_k \leq \Delta u_{max} \end{aligned} \tag{4.25}$$

There are of course also implementations of constraints for upper and lower bound of the absolute value of the control signal and output constraints. However, since no information about these constraints is known, these implementations will not be included in this thesis.

4.2 Kalman Filter

The Kalman filter was invented by R. E. Kalman in 1960, in a publication describing a discrete-data linear filtering solution. The Filter is based on linear stochastic difference equations. It estimates the states of a process at each time sample, called the time update, by using a form of feedback control in the form of (noisy) measurements, called the measurement update. The time update is responsible for estimating the next value of the current state and error covariance. The measurement update is responsible for calculating the current estimate of the state, in other words correcting the measured value.

4.2.1 State estimation

The Kalman filter algorithm used in this thesis is a discrete Steady State Kalman filter. The model used for the filter is deterministic in nature but is augmented with stochastic terms. The linear model 3.3 with the stochastic terms w_k and v_k is given as

$$\begin{aligned} x_{k+1} &= \mathbf{F}x_k + \mathbf{G}u_k + w_k \\ y_k &= \mathbf{C}x_k + v_k \end{aligned} \tag{4.26}$$

where w_k and v_k are defined as

$$\begin{bmatrix} w_k \\ v_k \end{bmatrix} \in N_{iid}\left(\begin{bmatrix} 0 \\ 0 \end{bmatrix}, \begin{bmatrix} \mathbf{Q} & 0 \\ 0 & \mathbf{R} \end{bmatrix}\right) \tag{4.27}$$

where $\mathbf{Q}$ and $\mathbf{R}$ are the process noise covariance and measurement noise covariance respectivly.

Measurement update

At each new time sample the residual or innovation error e_k is computed from the estimated output $\hat{y}_{k-1}$ and the measured output y_k

$$\begin{aligned} \hat{y}_{k-1} &= \mathbf{C}\hat{x}_{k-1} \\ e_k &= y_k - \hat{y}_{k-1} \end{aligned} \tag{4.28}$$

The Kalman gain $\mathbf{K}_{f,k}$ can be calculated as

$$\begin{aligned} \mathbf{R}_{e,k} &= \mathbf{C}\mathbf{P}_{k-1}\mathbf{C}' + \mathbf{R} \\ \mathbf{K}_{f,k} &= \mathbf{P}_{k-1}\mathbf{C}'\mathbf{R}_{e,k}^{-1} \end{aligned} \tag{4.29}$$

the corrected state estimate $\hat{x}_k$ and the error covariance $\mathbf{P}_k$ can be calculated from the Kalman gain $\mathbf{K}_{f,k}$

$$\begin{aligned} \hat{x}_k &= \hat{x}_{k-1} + \mathbf{K}_{f,k}e_k \\ \mathbf{P}_k &= \mathbf{P}_{k-1} - \mathbf{K}_{f,k}\mathbf{R}_{e,k}\mathbf{K}'_{f,k} \end{aligned} \tag{4.30}$$

Time update

The estimates of the state $\hat{x}_k$ is used to estimate the next evolution and is done after the new control signal have been calculated.

$$\begin{aligned} \hat{x}_{k+1} &= \mathbf{F}\hat{x}_k + \mathbf{G}u_k + \mathbf{G}_d d_k \\ \mathbf{P}_{k+1} &= \mathbf{F}\mathbf{P}_k\mathbf{F}' + \mathbf{Q}_k \end{aligned} \tag{4.31}$$

4.2.2 Filter Parameters

In a practical application, the measurement noise covariance $\mathbf{R}$ can be measured before the design of Kalman filter, by taking some off-line measurements. The process noise covariance Q is more difficult to determine before the filter is designed. As a designer one can try to guess the parameters of $\mathbf{Q}$ and $\mathbf{R}$, before applying the filter. In this thesis the neither the process or measurement noise is known, and the plant is view as a deterministic process. Here the ratio between $\mathbf{Q}$ and $\mathbf{R}$ will determine the amount of confidence that is placed either the model or the measurements. If $\mathbf{Q} >> \mathbf{R}$ means that the variance of the process could be large and the measurements are trusted more than the plant model. The values of the Kalman gains will be large and this will lead to a fast estimation, which is less robust to higher frequencies of noise. If $\mathbf{Q} << \mathbf{R}$ gives that the variance of the measurements are larfe, and the process model is trusted more. This case will have a small Kalman gain and the process will be estimated slower, however, is less sensitive to noise. [11, page 439]

4.2.3 Disturbance Estimation

The Kalman filter is excellent at estimating the states in the presence of noise that is zero-mean and white. However the accuracy degrades in the presences of non-zero mean disturbances, which as a result the controller will not be able to reject these disturbances. The Kalman filter needs to have disturbance estimation implemented. The goal of the disturbance estimation is to eliminate steady state errors in the controlled outputs. This will improve the closed loop robustness against disturbances and noisy measurements. The steady state error can be removed by having one or more integrators in the control loop. There are two most known methods to eliminate the steady state error. One is taking from 'classical' control theory, where as with a PI controller, the control objective is augmented with a integration of the tracking error. However this method leads to

extra tuning parameters, which means more computations, and that a anti-wind up algorithm may be needed[14]. The other method is to augment the estimator with integrating states, by using disturbance models as described in [5].
In this thesis the discrete linear model 3.3 is augmented with a disturbance model, in this case a constant non-zero disturbance is modelled. The resulting model for the Kalman filter results in

$$\begin{aligned} \begin{bmatrix} x_{k+1} \\ d_{k+1} \end{bmatrix} &= \begin{bmatrix} \mathbf{F} & \mathbf{G}_d \\ 0 & \mathbf{I} \end{bmatrix} \begin{bmatrix} x_k \\ d_k \end{bmatrix} + \begin{bmatrix} \mathbf{G} \\ 0 \end{bmatrix} u_k + \begin{bmatrix} w_k \\ \epsilon_k \end{bmatrix} \\ y &= \begin{bmatrix} \mathbf{C} & \mathbf{C}_d \end{bmatrix} \begin{bmatrix} x_k \\ d_k \end{bmatrix} + v_k \end{aligned} \tag{4.32}$$

where d_k is the disturbance vector, $\mathbf{G}_d$ is the input disturbance matrix and C_d is the output disturbance matrix. Usually the disturbance models are found through model identification techniques, however in research there are two general choices for the disturbance model [15].

- Choosing $G_d = 0$ and $C_d = \mathbf{I}$, is called the output disturbance model
- Choosing $G_d = \mathbf{I}$ and $C_d = 0$, is called the input disturbance model

The two choices can be combined such that the disturbance model will take into account of both input and output disturbances. The following assumptions are made based on [5], which have to be fulfilled for offset free control.

1. The pair $(\mathbf{F}, \mathbf{G})$ is controllable or at least is stabilizable.
2. The pair $(\mathbf{F}, \mathbf{C})$ is detectable.
3. The number of controlled variables nz, cannot be greater than the number of manipulated variables nu. $nz \leq nu$
4. The augmented system needs to be detectable. The matrix in 4.33 must have full column rank as stated in [5] and [16].

$$\begin{bmatrix} I - F & -G_d \\ C & C_d \end{bmatrix} \tag{4.33}$$

For condition 4 to be satisfied the number of disturbances must be equal or less than the number of measurements.

4.2.4 Disturbance Rejection

Given the disturbance estimate the state and input new steady state values are computed by solving the following equation

$$\begin{bmatrix} \mathbf{I} - \mathbf{F} & -\mathbf{G} \\ \mathbf{C} & \mathbf{0} \end{bmatrix} \begin{bmatrix} x_{ss} \\ u_{ss} \end{bmatrix} = \begin{bmatrix} \mathbf{G}_d d_k \\ -\mathbf{C}_d d_k \end{bmatrix} \tag{4.34}$$

where the new steady state values x_{ss} and u_{ss} are then substituted from the estimated states and input in the controller, which will drive the the system away from the effects of the disturbances.

$$\begin{bmatrix} x_{ss} \\ u_{ss} \end{bmatrix} = \Gamma_d \hat{d}_k \tag{4.35}$$

where Γ_d and Γ_R are determined by

$$\mathbf{\Gamma}_D = \begin{bmatrix} \mathbf{H}_{1,d} & \mathbf{C}_d & 0 & \cdots & 0 \\ \mathbf{H}_{2,d} & \mathbf{H}_{1,d} & \mathbf{C}_d & \ddots & \vdots \\ \mathbf{H}_{3,d} & \mathbf{H}_{2,d} & \mathbf{H}_{1,d} & \ddots & 0 \\ \vdots & \vdots & \vdots & \ddots & \vdots \\ \mathbf{H}_{N,d} & \mathbf{H}_{N-1,d} & \mathbf{H}_{N-2,d} & \cdots & \mathbf{H}_{1,d} \end{bmatrix} \tag{4.36}$$

where $\mathbf{H}_d$ are the impulse response coefficients of the system with respect to input and disturbance matrices

$$\mathbf{H}_{i,d} = \mathbf{C}_z \mathbf{F}^{i-1} \mathbf{G}_d \tag{4.37}$$

This changes the control formulation to incorporate the disturbance models and the controller will be able to calculate the optimal control signal for a system under disturbances. The control formulation can now be written as

$$\begin{aligned} \min_U \phi \quad &= \frac{1}{2} \sum_{k=1}^{N} \|z - r\|^2_{W_z} + \frac{1}{2} \sum_{k=0}^{N-1} \|\Delta u_k\|^2_{W_u} \\ \text{s.t.} \quad & \hat{x}_{k+1} = \mathbf{F}\hat{x}_k + \mathbf{G}u_k + \mathbf{G}_d \hat{d}_k \\ & z_k = \mathbf{C}_z \hat{x}_k \\ & y_k = \mathbf{C}_y \hat{x}_k + \mathbf{C}_d d_k \end{aligned} \tag{4.38}$$

CHAPTER 5

Applied Control

In this section, the design decisions that was made during the design of the model predictive controller will be presented. For the controller design, the model variables used are introduced and followed by the tuning strategy used in the design.

The complete controller design follows the sketch of figure 5.1, the reference r_K and the estimated measured controlled variables z_k will create the error signal e for the model predictive controller, which calculates the next control move Δu for the process. The output of the float zone process is measured and which is fed to the Kalman filter, that will estimate correct value and estimate the disturbances if there are any.

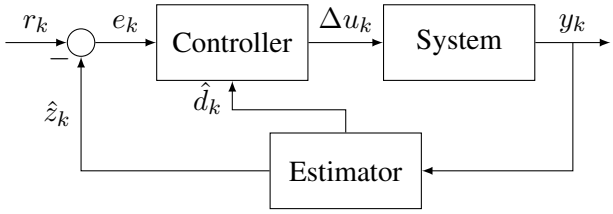

Figure 5.1: Control system structure

The control structure for the float zone process is as follows: The states x are defined as: The crystal rod radius R_C, The upper zone height h_F, the lower zone height h_C, the visible melt volume V_{vi}, the radius of the melt neck R_N, the voltage in the inductor U_{ind}, the melting rate of the feed rod v_{Me} and finally the crystallization rate of the crystal rod v_{Cr}. The measured variables y are the state variables, as all states are assumed to be measurable In the real application this is not the case. The manipulated variables u are the generator voltage U_{gen} and the pull rate of the feed rod v_F. The pull rate of the crystal rod is kept constant in steady state. This is done to prevent sudden pulls in the crystal, which can introduce dislocations in the crystal rod. The measured disturbance variable is the radius of the feed rod R_F. The angle of this rod is assumed constant $\alpha_F = 0$. The controlled variables are the crystal radius R_C and the lower zone height h_C. A summary of the structure can be seen in the list below.

- The state vector: $x = \begin{bmatrix} R_C & h_F & h_C & \phi_C & V_{vi} & R_N & U_{ind} & v_{Me} & v_{Cr} \end{bmatrix}^T$
- The measurement vector: $y = \begin{bmatrix} R_C & h_F & h_C & \phi_C & V_{vi} & R_N & U_{ind} & v_{Me} & v_{Cr} \end{bmatrix}^T$
- The input vector: $u = \begin{bmatrix} U_{gen} & v_F \end{bmatrix}^T$
- The measured disturbance vector: $d_m = \begin{bmatrix} R_F \end{bmatrix}^T$
- The controlled states vector: $z = \begin{bmatrix} R_C & h_C \end{bmatrix}^T$

The controller used in implementation for the rest of the thesis is a the input rate constrained MPC with weighted control moves. The MPC has the following structure and constraints.

$$\min_U \phi = \phi_z + \phi_{\Delta u} = \frac{1}{2}\sum_{k=1}^{N} \|z_k - r_k\|^2_{W_z} + \frac{1}{2}\sum_{k=0}^{N-1} \|\Delta u_k\|^2_{W_u} \tag{5.1}$$

$$\begin{aligned} &\text{s.t.} \\ x_{k+1} &= \mathbf{F}x_k + \mathbf{G}u_k + \mathbf{G}_{d_m} d_{m,k} \\ z_k &= \mathbf{C}_z x_k && k = 0, 1, ..., N-1 \\ y_k &= \mathbf{C}_y x_k && k = 0, 1, ..., N-1 \\ \Delta u_{min} &\leq \Delta u_k \leq \Delta u_{max} && k = 0, 1, ..., N-1 \end{aligned} \tag{5.2}$$

5.1 Controller Tuning

The goal of the final tuning is to resemble the controller response that could be used for implementation on the process at Topsil GlobalWafers A/S. The tuning of the closed loop response works by adjusting the weight matrices W_z and $W_{\Delta u}$ as well as the prediction horizon as it is stated in section 4, in order to achieve the desired performance of the system. Several methods are available when choosing a tuning strategy such as trial-and-error and Bryson's rule [11], which tunes the weight by using a normalisation of the maximum allowed values of the state values and input moves. The trial-and-error method was used in this thesis, as the maximum allowed values of the state and control moves are not known, however, some time domain specifications for a reference response, have been given by the supervisors from Topsil GlobalWafers A/S. The system is allowed to use about 20 minutes to settle at a new reference value, with an over dampened response, and the control action have to be limited to give a smooth input response.

As such several simulations are performed to analyse the impacts of the weights on the response of the float zone process, four cases are developed. The prediction horizon has been chosen to be $N = 180$ samples, with a sample time of 1 sample per. second. It could be argued that the prediction horizon could be chosen with a bigger horizon, however, this would increase the computational time for each time step, and the chosen sample time gives a stable response. In each case, four different tunings, denoted as (1), (2), (3) and (4) respectively, are analysed and the best

candidate is chosen to be kept constant in the next case.

The first case in figure 5.2 shows the tuning of the control moves with $W_{\Delta u}$, a reference is made on the crystal diameter D_C, while the lower zone height h_C is to be kept at the steady state value. The diagonal values of $W_{\Delta u}$ and W_z used for the control move are shown in table 5.1.

#	$W_{\Delta u}$		W_z	
	U_{gen}	v_F	R_C	h_C
1	1	1	1	1
2	1e3	1e3	1	1
3	1e6	1e6	1	1
4	1e9	1e9	1	1

Table 5.1: First case of four iteration of Tuning parameters for figure 5.2.

In sub figure 5.2a the reference change response is shown for the four different tunings. By studying the control signals in sub figure 5.2c and 5.2d it can be seen that tuning (1) and (2) fluctuate wildly and these tunings are easily discarded, however, control actions of tuning (3) and (4) is almost indistinguishable. Subfigure 5.2b shows a better picture of (3) and (4). Here (4) is not able to move the lower zone height to the reference point. As such tuning (3) is chosen as the best candidate for the input weights.

The second case shows the tuning of the controlled variable, D_C the crystal diameter with W_z. A reference step change is made in the crystal diameter reference, while the lower zone height is to be kept at the steady state value. The weights of the tuning are shown in table 5.2 which are used in simulations shown in figure 5.3. The weights on the crystal radius are changed in each iteration and the lower zone height is kept constant. In sub figure 5.3c it can be seen the tuning (1) and (2) still has a very aggressive response.

#	$W_{\Delta u}$		W_z	
	U_{gen}	v_F	R_C	h_C
1	1e6	1e6	1e-1	1
2	1e6	1e6	1e-2	1
3	1e6	1e6	1e-3	1
4	1e6	1e6	1e-4	1

Table 5.2: Second case of four iterations of tuning parameters.

The third case shows the tuning of the controlled variable h_C, the lower zone height, with W_z. A reference step change is made in the crystal diameter reference, while the lower zone height is to be kept at the steady state value. The weights of the tuning are shown in table 5.3 which are

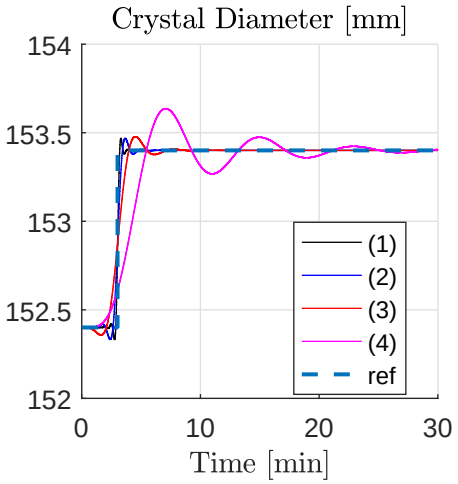

(a) Reference change response for the crystal diameter D_C.

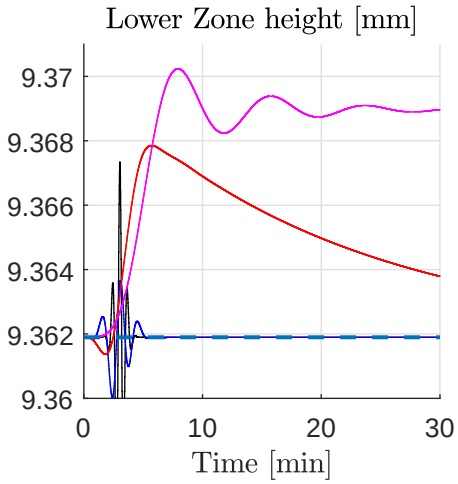

(b) The response of the lower zone height h_C.

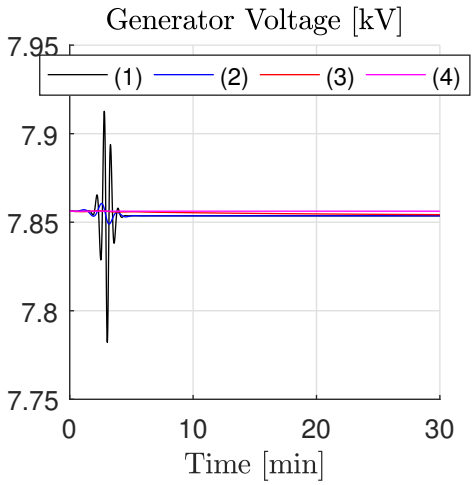

(c) The control signal for the generator voltage U_{gen}.

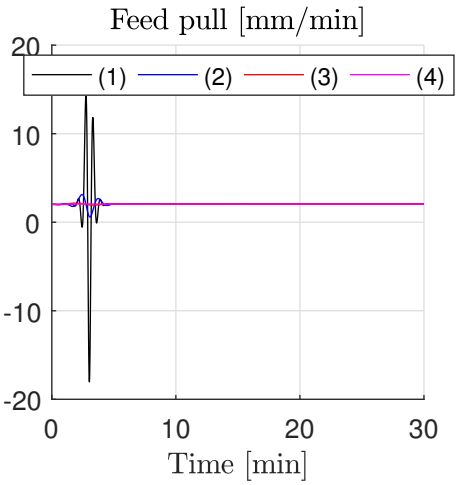

(d) The control signal for the feed pull rate v_F.

Figure 5.2: Four different tunings are shown, named 1 to 4. Here the weight of the control move are changed iteratively

used in simulations shown in figure 5.4. The weights on the lower zone height are changed in each iteration.

The control action of the generator voltage in sub figure 5.4c all show reasonable responses. The control action of the feed pull rate in sub figure 5.4d tuning (1) still gives an oscillating response, and tuning (2) and (3), a more smooth response. In sub figure 5.4a tuning (3) and (4) have a smooth over damped response which was the goal of the tuning strategy. However tuning (4), has a slower settling time. Tuning (3) is chosen as the best tuning.

Finally, the weights are changed slightly to give the final response as shown in figure 5.5. The final weights used are shown in 5.4, and will be used through the rest of the thesis.

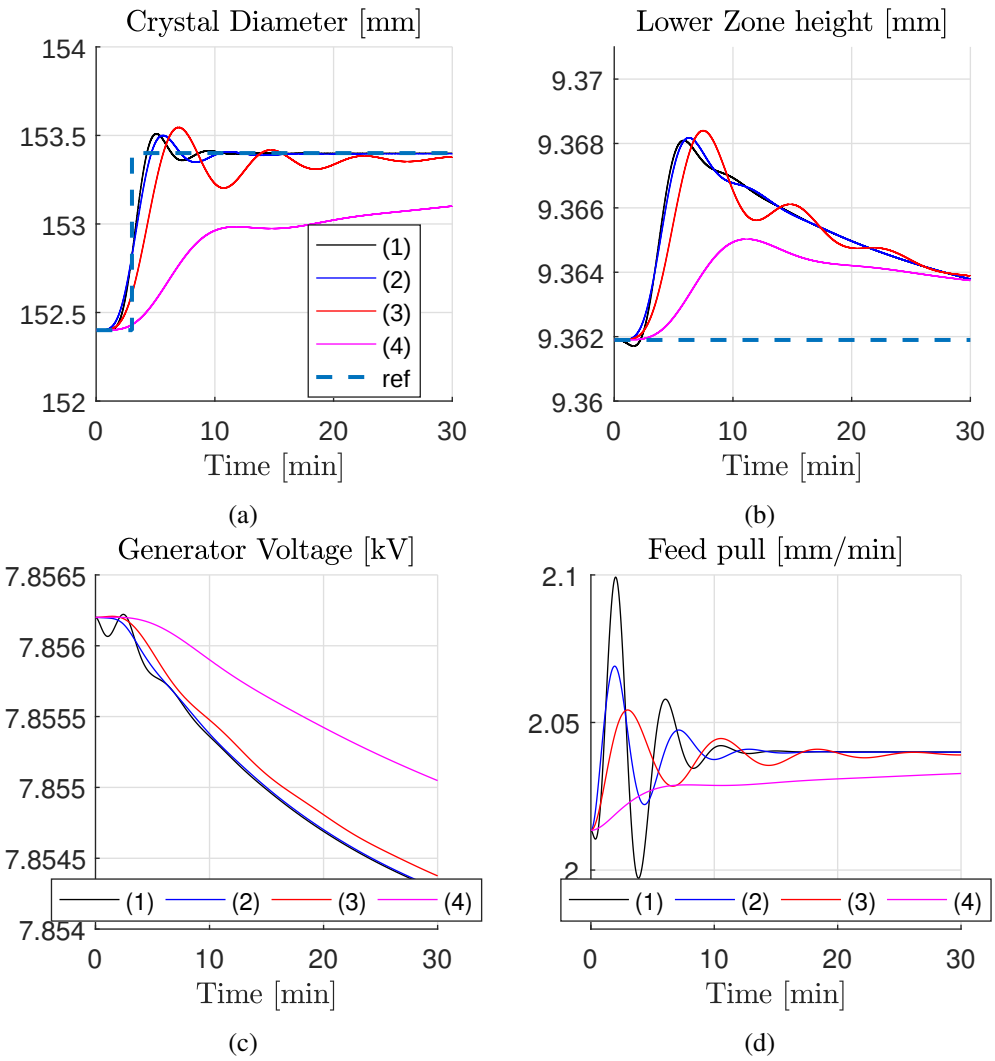

Figure 5.3: Four different tunings are shown, named 1 to 4. Here the weights of the crystal radius are changed iteratively

#	$W_{\Delta u}$		W_z	
	U_{gen}	v_F	R_C	h_C
1	1e6	1e6	1e-3	1e1
2	1e6	1e6	1e-3	1e2
3	1e6	1e6	1e-3	1e5
4	1e6	1e6	1e-3	1e7

Table 5.3: Third case of four iterations of tuning parameters.

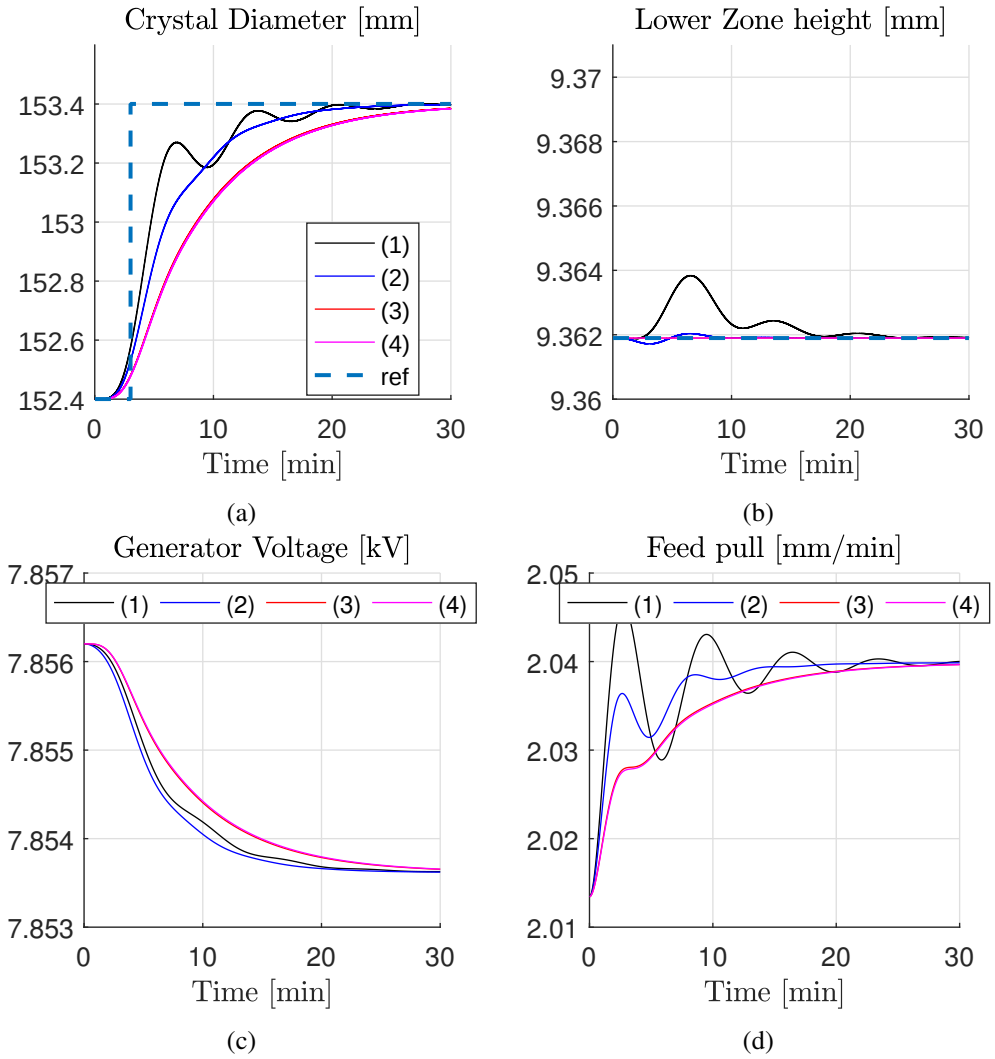

Figure 5.4: Controller tuning of the lower zone height

#	$W_{\Delta u}$		W_z	
	U_{gen}	v_F	R_C	h_C
1	1e6	1e6	2.5e-3	1e5

Table 5.4: Forth case of iterations of tuning parameters for the model predictive controller. This table is matched with figure 5.5.

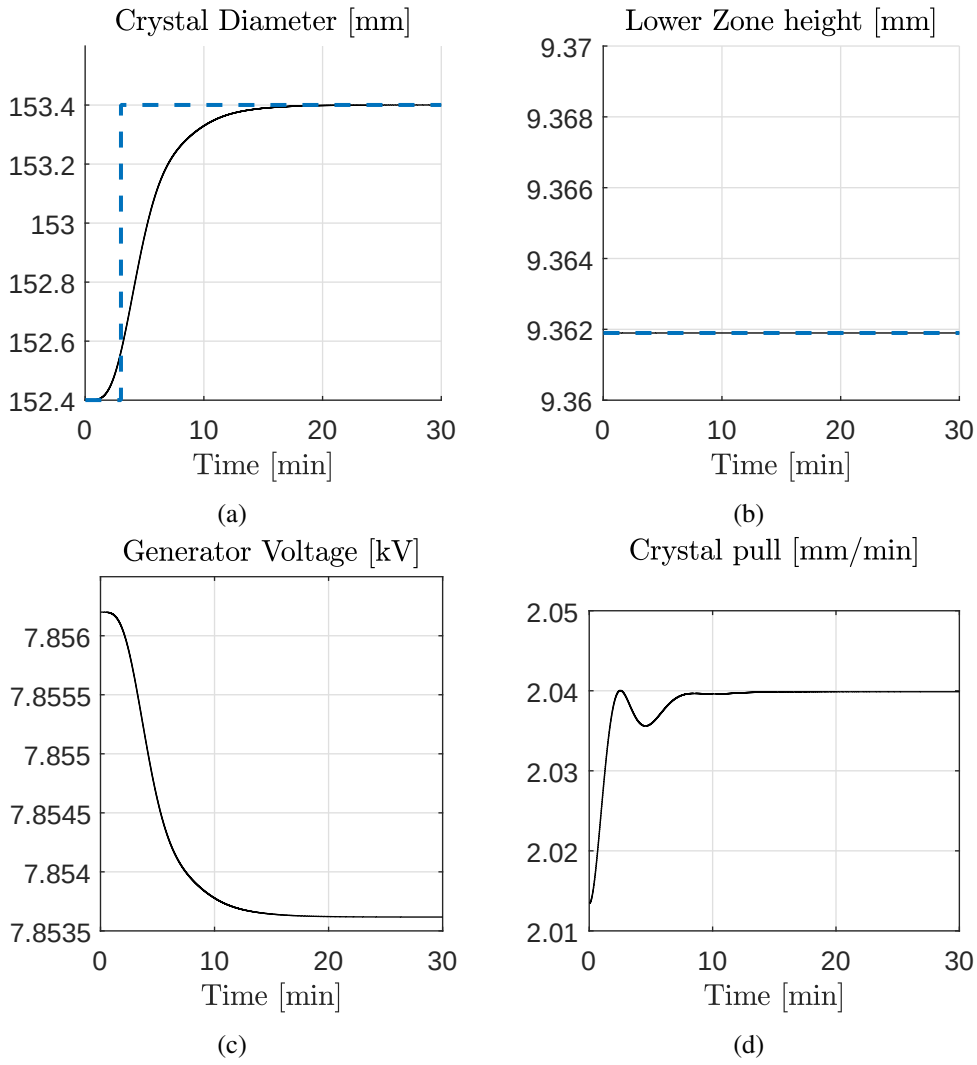

Figure 5.5: Final Tuning of the controller

CHAPTER 6

Results of the offset free Control

This chapter deals with the application of the presented offset free control method on the non linear float zone process presented in chapter 2. The performance of the system in rejecting non-zero mean constant disturbances will be evaluated, as the goal of the offset free control is to keep the crystal diameter at the reference in the presences of disturbances. Firstly, the system will be evaluated without disturbances with a change in reference. Secondly the system will be simulated with different disturbances. The system will be evaluated with a disturbance in the inputs, namely in the generator voltage, the feed pull rate and the crystal pull rate to simulate faulty actuators. Then the system will be evaluated with a change in the poly crystal radius, which will be viewed as a unknown disturbance. Lastly, the system will be evaluated with disturbances in the state variables, this will simulate a model mismatch between the non-linear system and the linear model.

6.1 Summary: Results of Model Analysis

The eigenvalues of the linear model at the chosen operation point shows that there are repeated zero eigenvalues $\lambda = 0$ in the uncontrollable subspace. This results in a subspace of uncontrollable behaviour if those modes are excited. This means for the design of the controller that it is only valid if these states are not excited. As the scope of the thesis is not to remodel the given model, these uncontrolled eigenvalues cannot be made controllable, by introducing new inputs.
This means for that for the offset free control that there are some disturbances that the controller is not able to reject and the closed loop response might stable in the controlled variables, with a offset error, and unstable in some of the states as the controller will continuously try to bring the controlled variables to steady state.

6.2 Application of the Offset Free Control

This section deals with the application of the offset free control on the non linear model. The offset free control consists of the linear model based predictive controller and a Kalman filter

that estimates the size of the disturbances which the controller uses to remove the effect of the disturbances and move the system to the steady state values. The disturbances are considered to have a non zero mean with zero variance. The system will be evaluated by examining the controlled outputs, the manipulated variables and the constraints imposed on the manipulated variables, and discussing their responses to the disturbances.

The offset free controller is designed with the control formulation stated in equation 6.1 that is subject to equation 6.2.

$$\min_{U} \phi = \phi_z + \phi_{\Delta u} = \frac{1}{2}\sum_{k=1}^{N} \|z_k - r_k\|^2_{W_z} + \frac{1}{2}\sum_{k=0}^{N-1} \|\Delta u_k\|^2_{W_u} \tag{6.1}$$

$$\begin{aligned} &\text{s.t.} \\ x_{k+1} &= \mathbf{F}\hat{x}_k + \mathbf{G}u_k + \mathbf{G}_d\hat{d}_k \\ z_k &= \mathbf{C}_z\hat{x}_k && k = 0, 1, ..., N-1 \\ y_k &= \mathbf{C}_y\hat{x}_k + \mathbf{C}_d\hat{d}_k && k = 0, 1, ..., N-1 \\ \Delta u_{min} &\leq \Delta u_k \leq \Delta u_{max} && k = 0, 1, ..., N-1 \end{aligned} \tag{6.2}$$

where are the system matrices F, G, C_z and C_y, found by the linearisation method described in 3.2 and the disturbances matrices G_d and C_d are defined as identity matrices and the estimated disturbance vector $\hat{d}_k$ defined as a $n_d \times 1$ vector where $n_d = n_y$, n_y is the number of measured outputs and n_d is the number of integrating disturbances. The diagonal weight matrices used have been determined in section 5.1. The constraints on Δu are $\Delta u_{min} = 0.05\text{kV}\,\text{min}^{-1}$ and $\Delta u_{max} = 0.05\text{mm}\,\text{min}^{-1}$.

The static steady state Kalman filter is designed with regards to section 4.2.2 with the following model

$$\begin{aligned} \begin{bmatrix} \hat{x}_{k+1} \\ \hat{d}_{k+1} \end{bmatrix} &= \begin{bmatrix} \mathbf{F} & \mathbf{G}_d \\ 0 & \mathbf{I} \end{bmatrix} \begin{bmatrix} \hat{x}_k \\ \hat{d}_k \end{bmatrix} + \begin{bmatrix} w_k \\ \epsilon_k \end{bmatrix} \\ \hat{y}_k &= \begin{bmatrix} \mathbf{C}_y \mathbf{C}_d \end{bmatrix} + v_k \end{aligned} \tag{6.3}$$

where the covariance matrix of the model noise $Q_{w,\epsilon}$ is chosen with large diagonal variances and the covariance of the measurements R_v is chosen to be a diagonal matrix with much lower values of Q. The numerical values are $Q_{w,\epsilon} = 1$ and $R_v = 0.001$. Thus, a fast estimation of the states and disturbances is achieved.

6.2.1 Disturbance in the Generator Voltage

Figure 6.1 on the following page shows the response of the controlled system with a disturbance on the generator voltage that has a mean of 0.1% of the nominal steady state value which corresponds to the generator is delivering 0.78 V more than expected. A open loop response with a change in the generator voltage will result in a transient response of the crystal diameter that is asymptotically stable around the steady state, however the lower zone height will move toward a new steady state value that is defined by equation 2.10 and 2.42.
Sub figure 6.1a and 6.1b the responses of the crystal diameter and the lower zone height. It can be seen that both variables experience a temporary effect of the disturbance in the generator voltage, however the controller rejects the disturbance such that both variables settles at their steady state values after about 20 minutes after the disturbance is introduced. In sub figure 6.1c the disturbance enters after 5 minutes (red stripped line), the controller (blue line) then starts rejecting the disturbance by lowering the generator voltage. The yellow line shows the input that the system experiences, which is a combination of the disturbance and the control signal. The feed pull rate in sub figure 6.1d reacts to the change in lower zone height introduced by the change in generator voltage. The designed controller is able to completely reject a disturbance in the generator voltage.

Figure 6.2 on page 51 shows the disturbance in the generator and the estimated disturbances affecting the states in the system. It is clearly seen that there are estimation errors. This is caused by two factors. First the non-linearities that cannot be captured by the linear disturbance model and that the disturbance model is not meant to model the disturbances accurately, since adding the a disturbance that does not occur in the plant introduces model mismatch. However the integrating disturbance can be used in the control action for offset free control, which can clearly be seen in sub figures 6.1a and 6.1b.

6.2.2 Disturbance in the Pull Rates

Figure 6.3 on page 52 shows the response of the controlled system with a disturbance on the feed pull rate with a mean of 0.1% of steady state, which results in the feed pull rate is increased 0.0021 mm per. min. A open loop response with a change in the feed pull rate would show a that the crystal diameter and lower zone height would increase or decrease and move to a new equilibrium point due to the increase or decrease of material in the system.

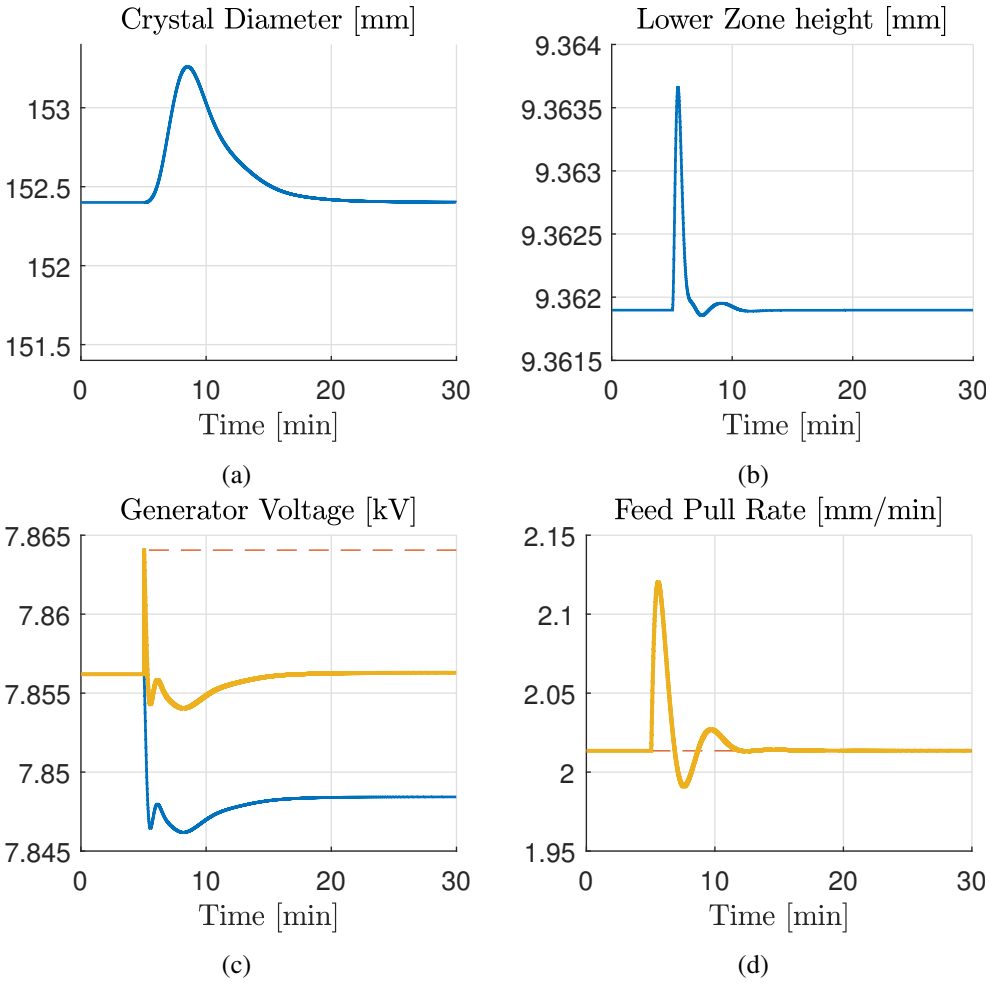

Figure 6.1: System response to a disturbance in the generator voltage. In sub figure c and d, the red striped line is the real value of the disturbance, the yellow thick line is the true input as viewed by the system, the blue line is the control signal.

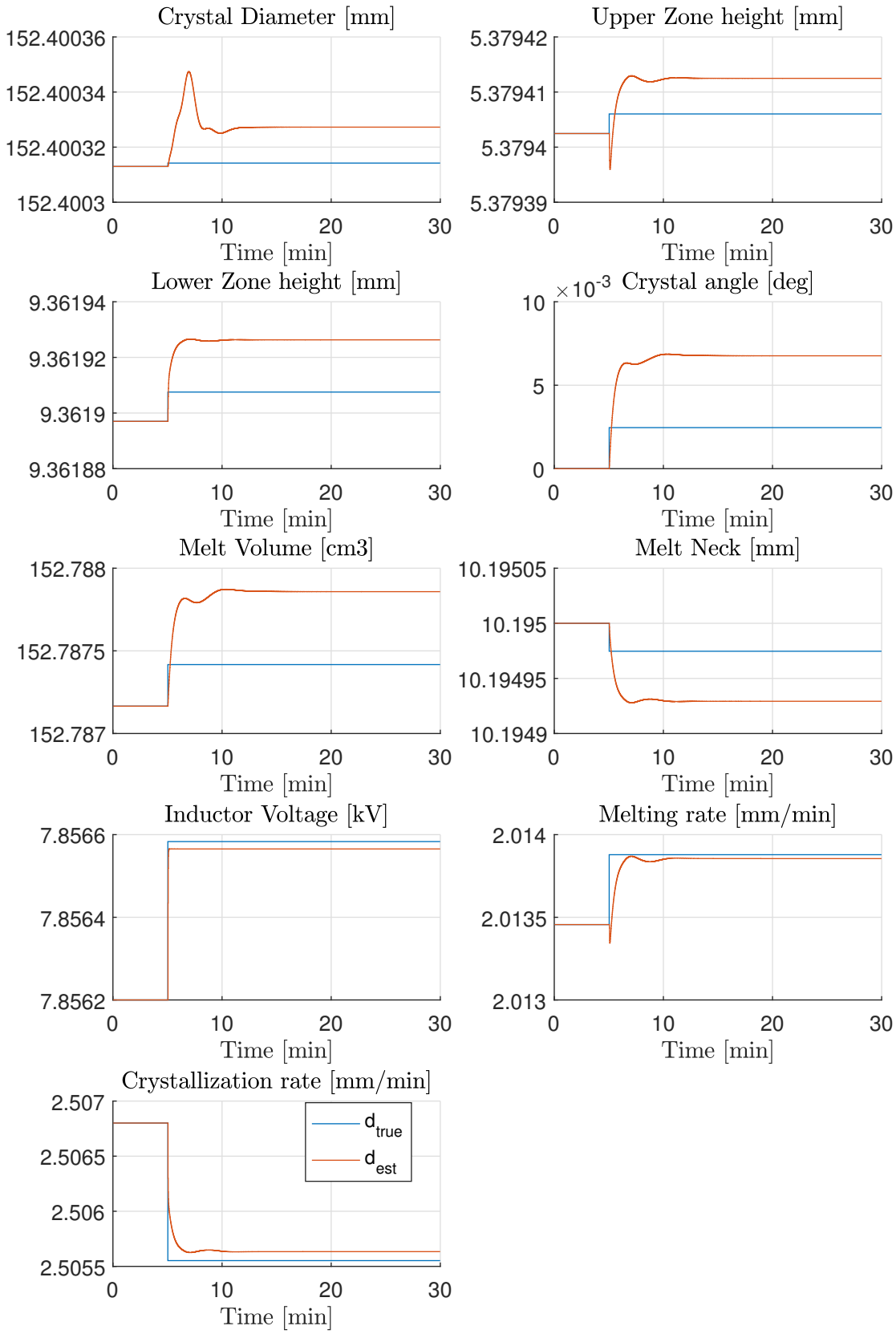

Figure 6.2: Disturbance estimate of a disturbance in the generator voltage

In sub figure 6.3a and 6.3b a small error occurs on the crystal diameter and the lower zone height. The error in the crystal diameter is quickly rejected, the lower zone height however, has a slower rejection, but the disturbance is completely rejected. It can be seen in 6.3d that the disturbance (red line) is rejected by the controller (blue line) by lowering the feed pull rate. This seen by the system as a transient response that settles at the same steady state value as before the disturbance, which will move the lower zone height back to its steady state.

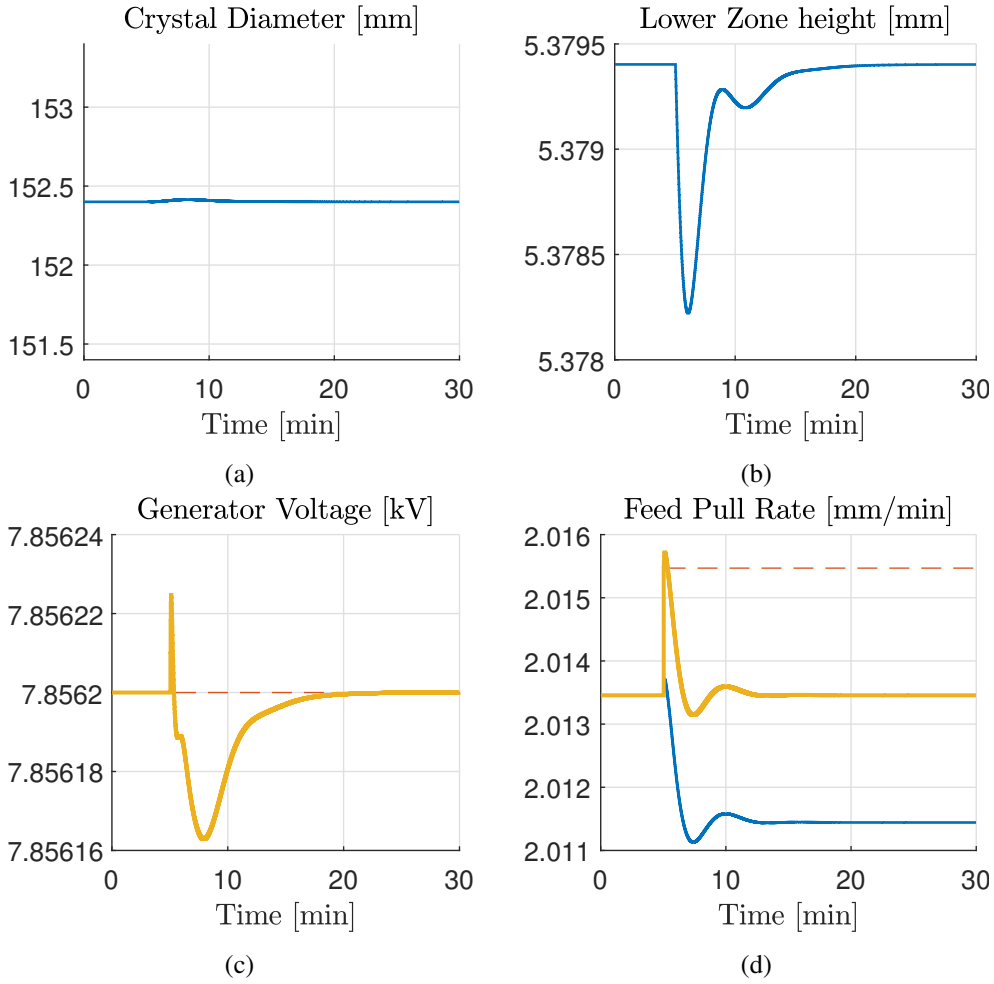

Figure 6.3: System response to a disturbance in the feed pull rate. In sub figure c and d, the red striped line is the true value of the disturbance, the yellow thick line is the true input as viewed by the system, the blue line is the control signal.

Figure 6.4 on the next page shows the response of the controlled system with a disturbance on the crystal pull rate with a mean of 0.1% of steady state, which results in a increased pull rate of 0.0025 mm/min. A open loop response with a step change in the crystal pull rate would show a increase or decrease of the crystal diameter and a increase or decrease of the lower zone height, as the crystal would see a sudden difference in the crystallization rate. The system would however stabilize to the new crystal pull rate.

In sub figure 6.4a it shows that the crystal diameter can be stabilized and the offset is removed.

However, in sub figure 6.4b the lower zone height has a non zero offset. This is caused by the restriction on the controller that the crystal pull rate cannot be changed by the controller during this phase. The controller cannot fully remove the effect of the disturbance by only changing the generator voltage and feed pull rate as one of the uncontrollable eigenvalues have been excited.

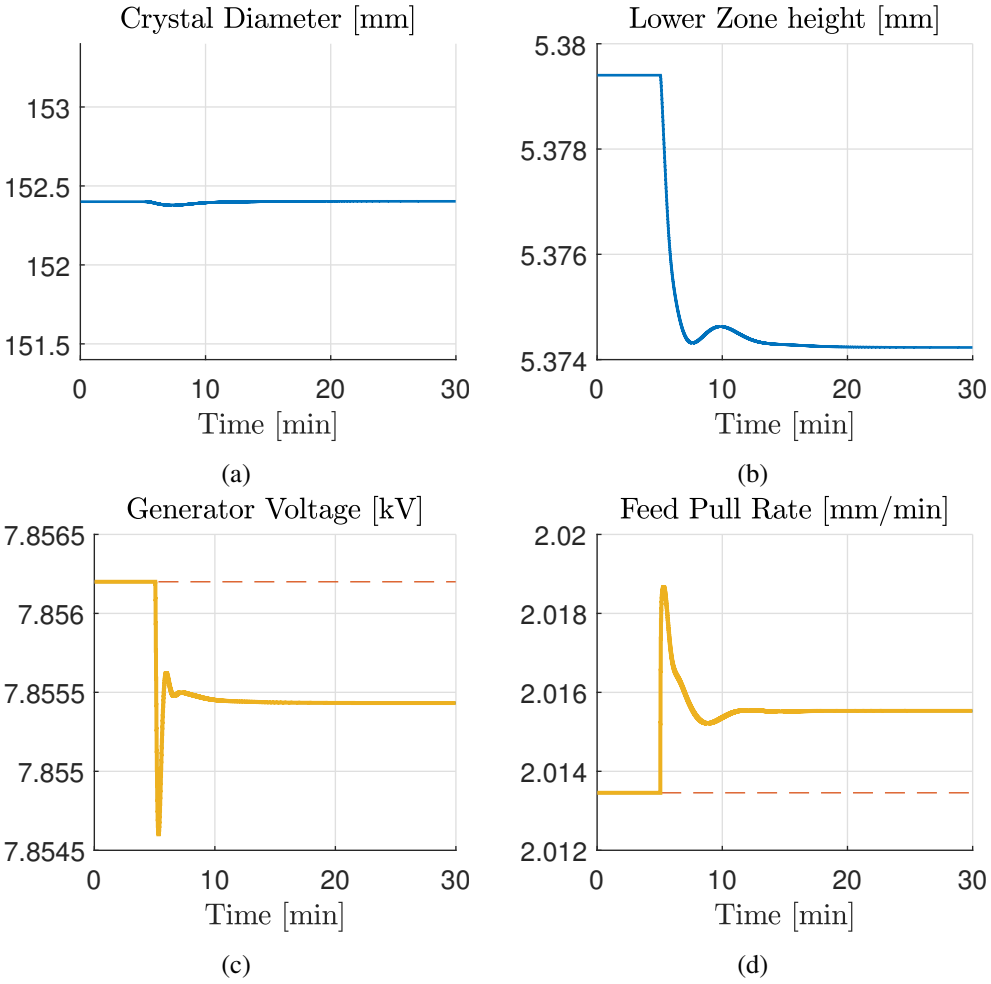

Figure 6.4: System response to a disturbance in the crystal pull rate.

6.2.3 Model Mismatch in Crystal Angle

Figure 6.5 on the following page shows the response of the controlled system with a disturbance on the crystal angle with a mean of $0.0057°$, which would simulate a model mismatch. A open loop response would show a increasing crystal diameter, which would increase the diameter of the crystal. Sub figure 6.5b shows that the controller is not able to keep the lower zone height at its steady state, when a disturbance enters in the crystal angle. However, it is able to reject the offset in the crystal diameter.

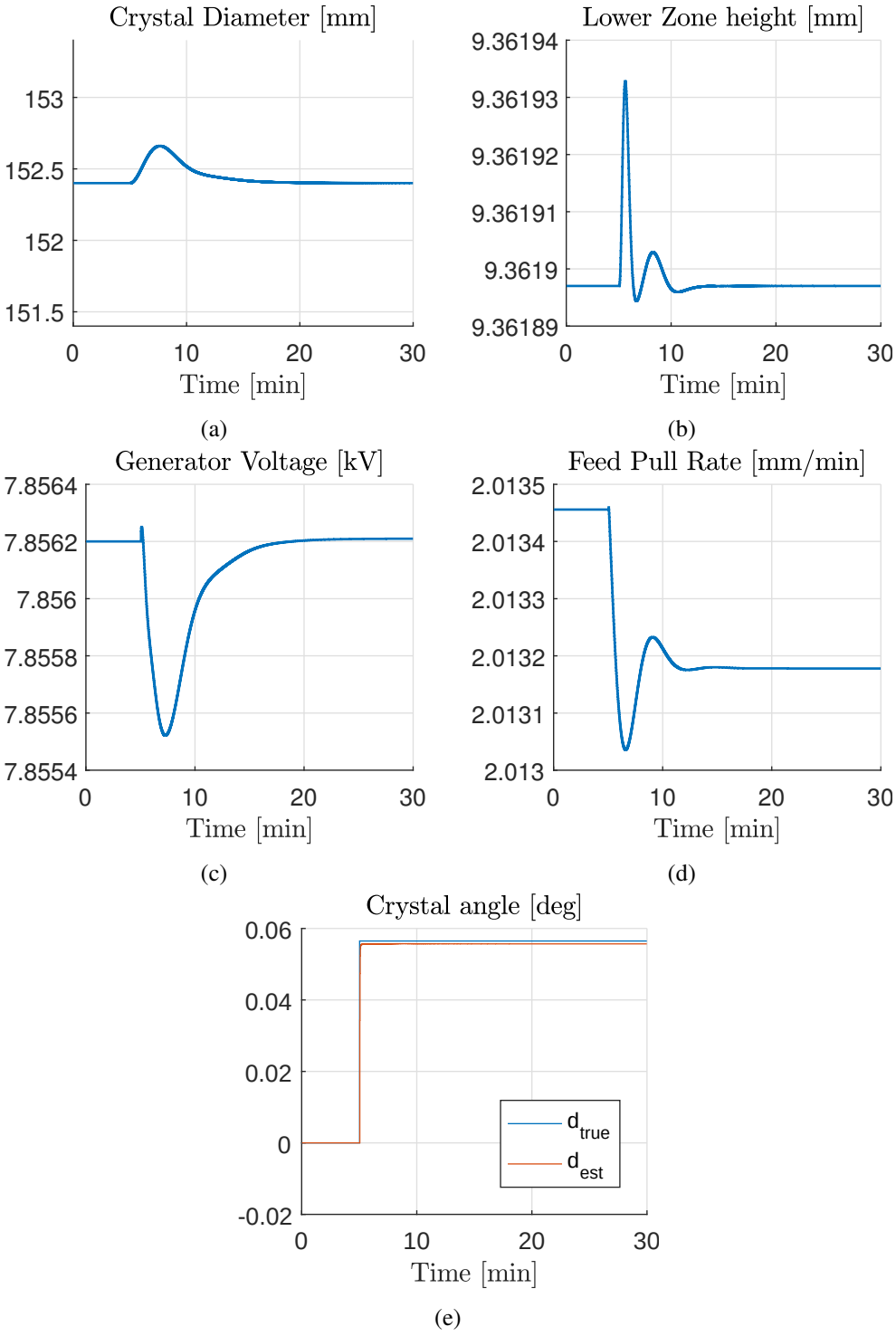

Figure 6.5: System response to a disturbance in the crystal angle.

6.2.4 Feed Rod Diameter Disturbance

Figure 6.6 shows the response of the controlled system with a disturbance on the feed crystal rod diameter, to show that the diameter of the poly crystal rod can fluctuate. A change in the diameter will change the volume of melt in the system. Sub figure 6.6a shows that the controller is able to reject the disturbance and move the crystal diameter to a zero offset. However, as previously the in lower zone height settles with a small offset as seen in sub figure 6.6b.

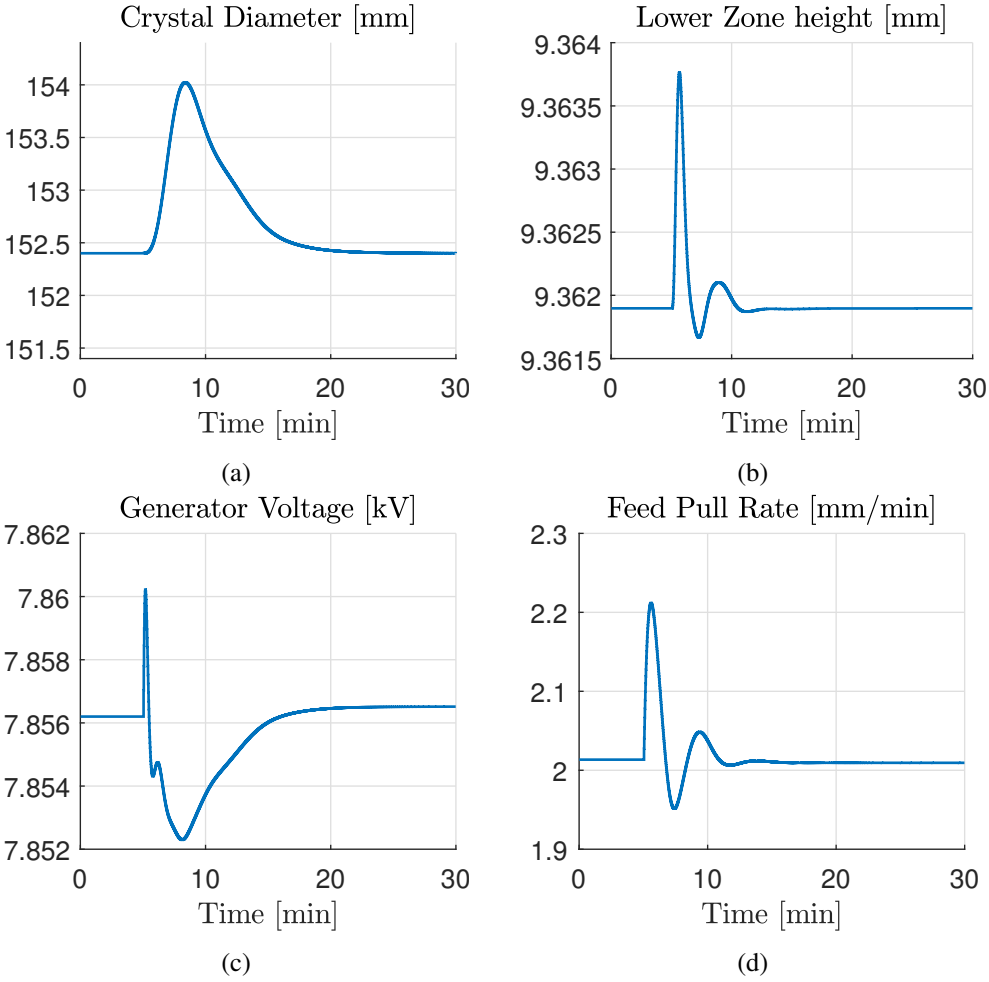

Figure 6.6: System response to a disturbance in the radius of the poly rod.

CHAPTER 7

Conclusions and Future work

7.1 Conclusion

In summary, this thesis investigated the possibility of using a linearised model of the float zone process described in Werner [1] to design a offset free model based predictive controller.

A non-linear model was given and was analysed by step responses to be able to understand the behaviour of the float zone system. By using a Jacobian linearisation method around a given operation point a linear time invariant model was found. The model was then simulated against the non-linear to verify that it could accurately be used to model the system. Then a stability was performed on the linear model. It was found that the model is marginally stable around the operation point. A controllability and observability analysis was then performed. The system was found not to be fully controllable, which means some of the states in the system cannot be controlled, however the uncontrollable states was found to be marginally stable. The system was found to fully observable, based on the assumption that all states could be measured in order to simplify the control problem.

A model predictive controller was designed on the basis of the linear model. This controller was chosen for its natural ability to optimally calculate control inputs for multi input multi output systems and keep the system within boundaries . The controller was designed to control the mono-crystal diameter and the distance between the solid part of the mono-crystal and the inductor and to be able to track reference changes. The controller was detuned, the crystal pull rate was removed as a manipulated variable, and the weights on the states and the inputs was designed such that only smooth control actions, that would not activate the constraints, could be taken and such that a reference change would result in a smooth increase in the crystal diameter over about 20 minutes.

A disturbance estimator was proposed and designed. A Kalman filter was used to estimate the disturbances, by augmenting the original linear model with a disturbance model. The disturbance model was chosen to both be able to estimate disturbances in the inputs and outputs of the system.

The model design of the disturbance estimator was kept as simple identity matrices. The estimated disturbances was given to the controller such that it reject the disturbances and remove the offset errors in the controlled outputs.

The disturbance estimator and controller was combined and different disturbances was introduced into the system. The controller was able to completely reject disturbances in the controlled variables and return them to their steady state values. However, the controller showed a degraded performance when disturbances was introduced as model mismatches or a disturbance in mono-crystal pull rate. It was shown that in the tested cases the offset could be removed in the crystal diameter, at the expense of the lower zone height having a offset.

7.2 Further study

Further study of the design of the disturbance models could be conducted in order to achieve better results. The Uncontrollable zero eigenvalues should also receive a deeper study, to see if they really are zero eigenvalues or if this is a modelling issue.

Bibliography

[1] Nico Werner. *Analysis and Automation of the Crucible-free Floating Zone (FZ) Growth of Silicon Crystals*. PhD thesis, 2014.

[2] Masood Askari, Mahmoud Moghavvemi, Haider A F Almurib, and K. M. Muttaqi. Multivariable Offset-Free Model Predictive Control for Quadruple Tanks System. *IEEE Transactions on Industry Applications*, 52(2):1882–1890, 2016.

[3] Audun Faanes and Sigurd Skogestad. Offset-free tracking with MPC with model mismatch : Experimental results. (1):1–14, 2005.

[4] Murali R. Rajamani, James B. Rawlings, and S. Joe Qin. Achieving state estimation equivalence for misassigned disturbances in offset-free model predictive control. *AIChE Journal*, 55(2):396–407, 2009.

[5] Gabriele Pannocchia and James B Rawlings. Disturbance models for offset-free model predictive control,. *AIChE Journal*, 49(2):426–437, 2003.

[6] Kenneth R. Muske and Thomas A. Badgwell. Disturbance modeling for offset-free linear model predictive control. *Journal of Process Control*, 12(5):617–632, 2002.

[7] Sune Duun, Anne Nielsen, Christian Hendrichsen, Theis Sveigaard, Ole Andersen, Jarosław Jabłoński, and Leif Jensen. Application Note Neutron Transmutation Doped (Ntd) Silicon for High Power Electronics. (October):1–12, 2013.

[8] Anke Lüdge, Helge Riemann, Michael Wünscher, Günter Behr, Wolfgang Löser, Andris Muiznieks, and Arne Cröll. Floating Zone Crystal Growth. In Thierry Duffar, editor, *Crystal Growth Processes Based on Capillarity*, pages 203–275. 2010.

[9] Werner Zulehner. Historical overview of silicon crystal pulling development, 2000.

[10] S. R. Coriell and M. R. Cordes. Theory of molten zone shape and stability. *Journal of Crystal Growth*, 42(C):466–472, 1977.

[11] Elbert Hendricks, Ole Jannerup, and Paul Haase Sorensen. *Linear Systems Control*, volume 53. 2013.

[12] Nonlinear Systems In, Aviation Aerospace, and Aeronautics Astronautics. Nonlinear Systems - second Edition. In *Journal of Climate J Clim Vol 18*, volume 18, pages 23–33. 2002.

[13] J. M. Maciejowski. *Predictive control: with Constraints*. Pearson Education Limited, 2002.

[14] John Bagterp Jørgensen. *Moving Horizon Estimation and Control*. PhD thesis, 2004.

[15] Parsa Rahmanpour, Morten Hovd, and John Atle Bones. *Nonlinear state estimation in the Czochralski process*, volume 19. IFAC, 2014.

[16] Francesco Borrelli and Manfred Morari. Offset free model predictive control. *Proceedings of the IEEE Conference on Decision and Control*, pages 1245–1250, 2007.

List of Figures

List of Tables

Appendices

Appendix A: Open Loop Responses

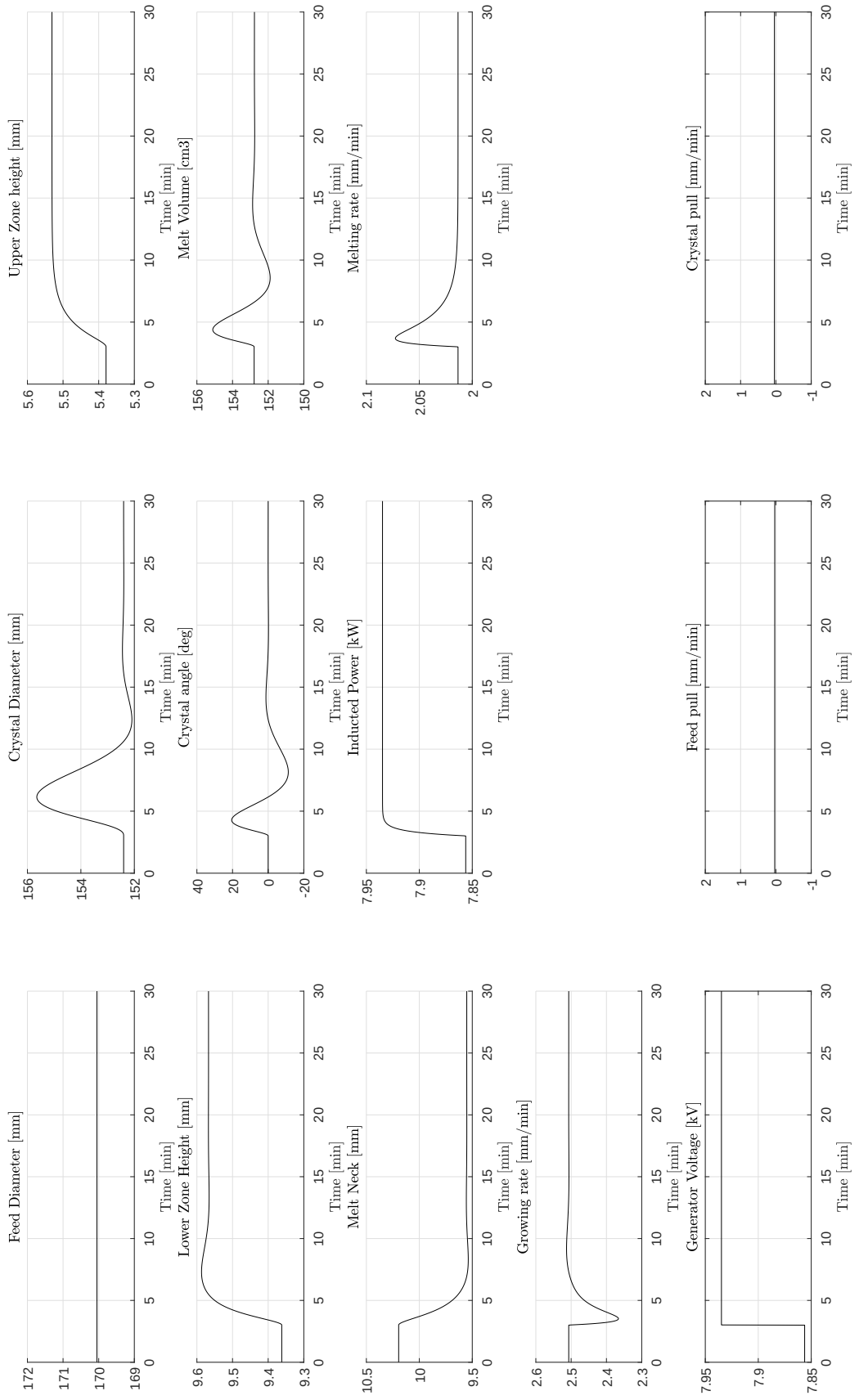

Figure 1: Open loop response to a input change in the generator voltage

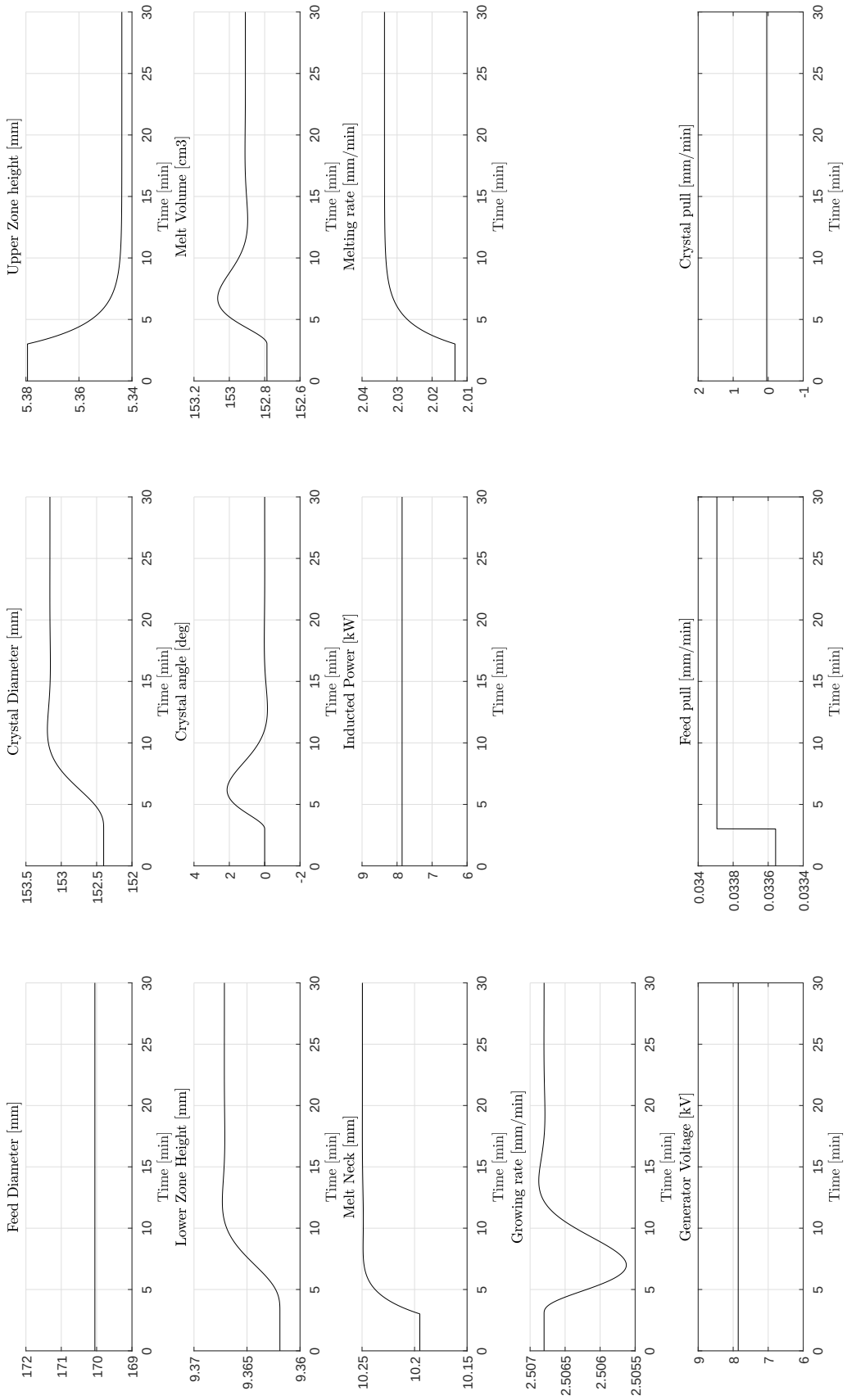

Figure 2: Open loop response to a input change in the feed pull rate

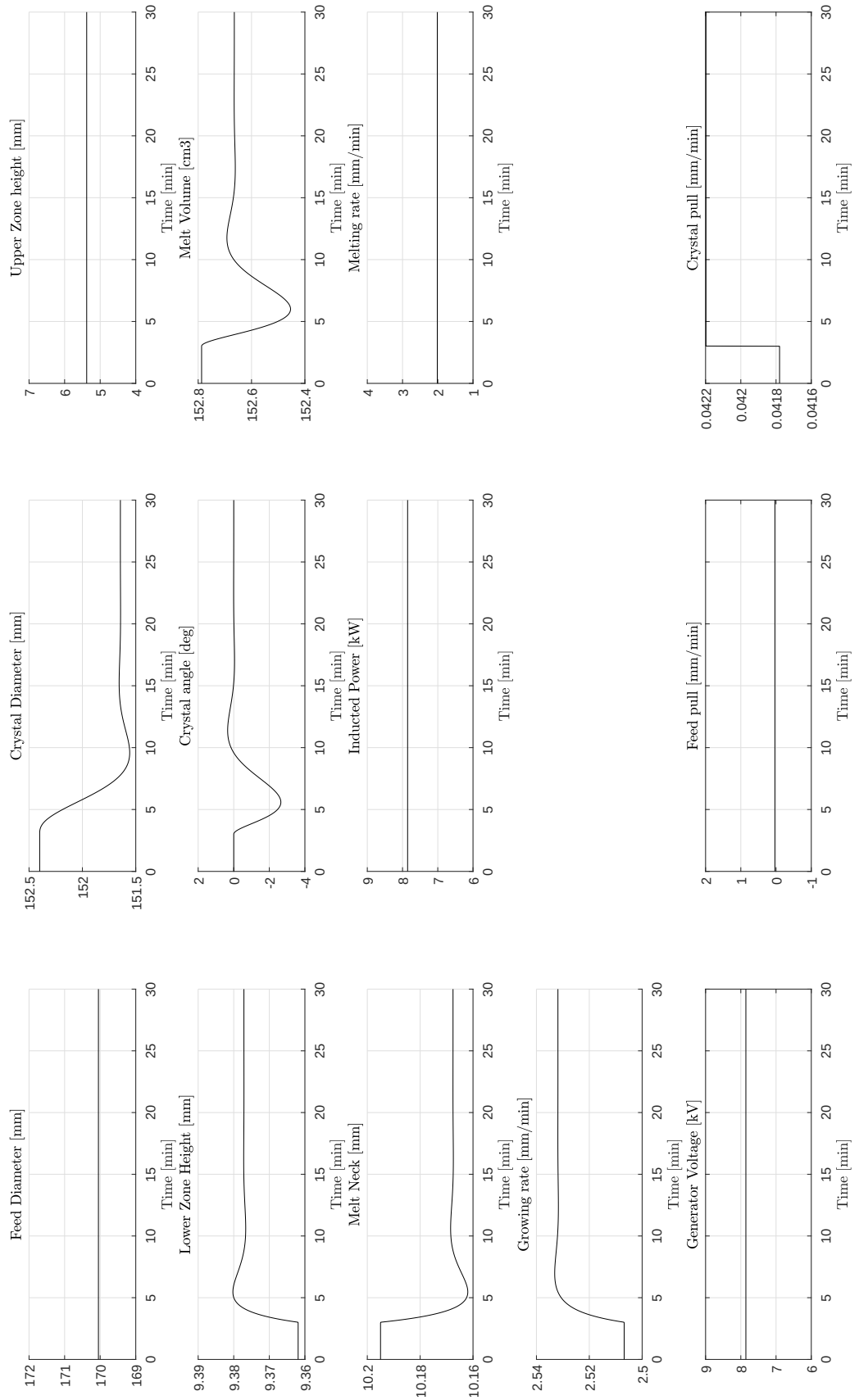

Figure 3: Open loop response to a input change in the crystal pull rate

Appendix B: Closed Loop Responses

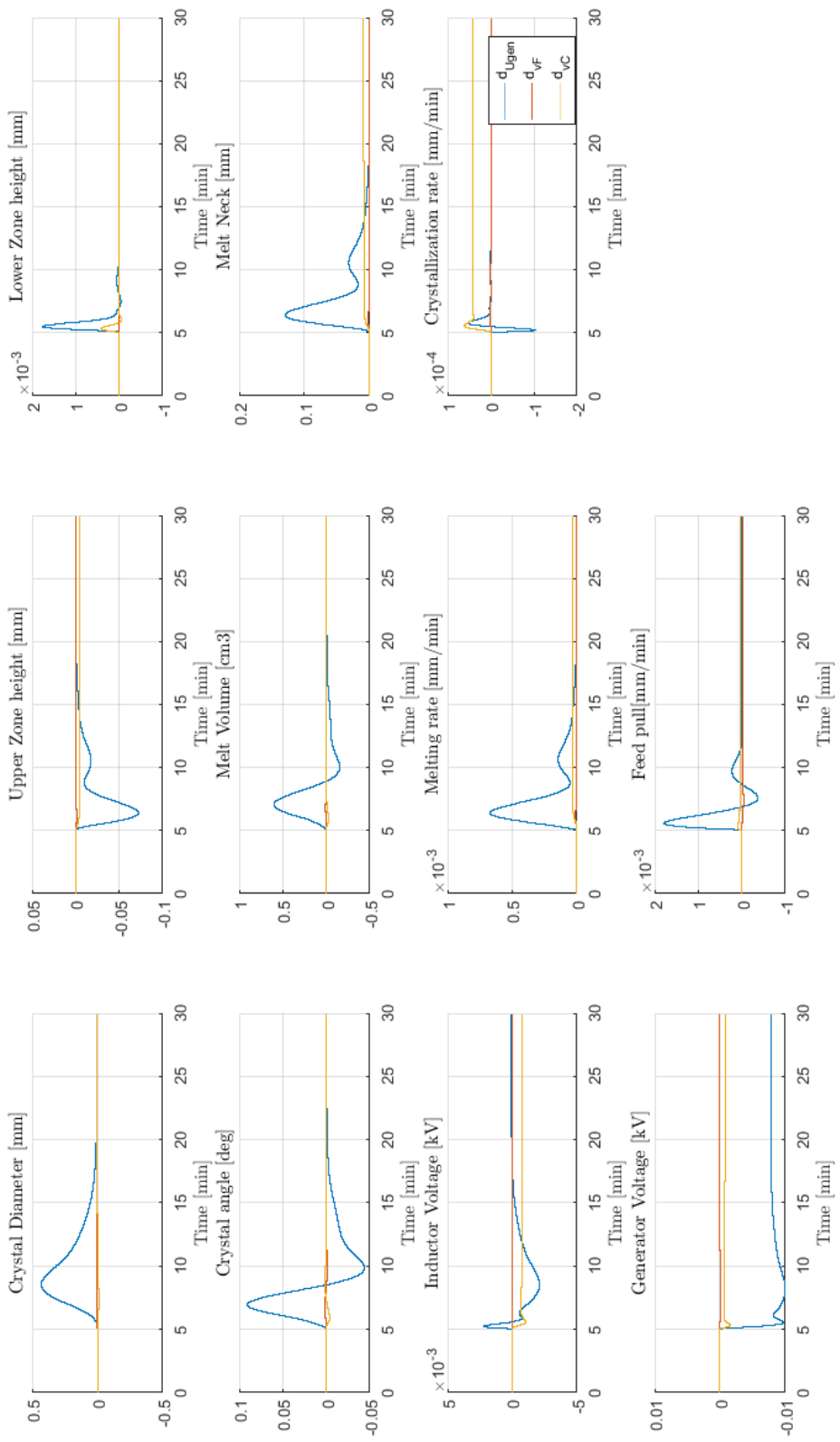

Figure 4: Figure of all states, with the three different input disturbances

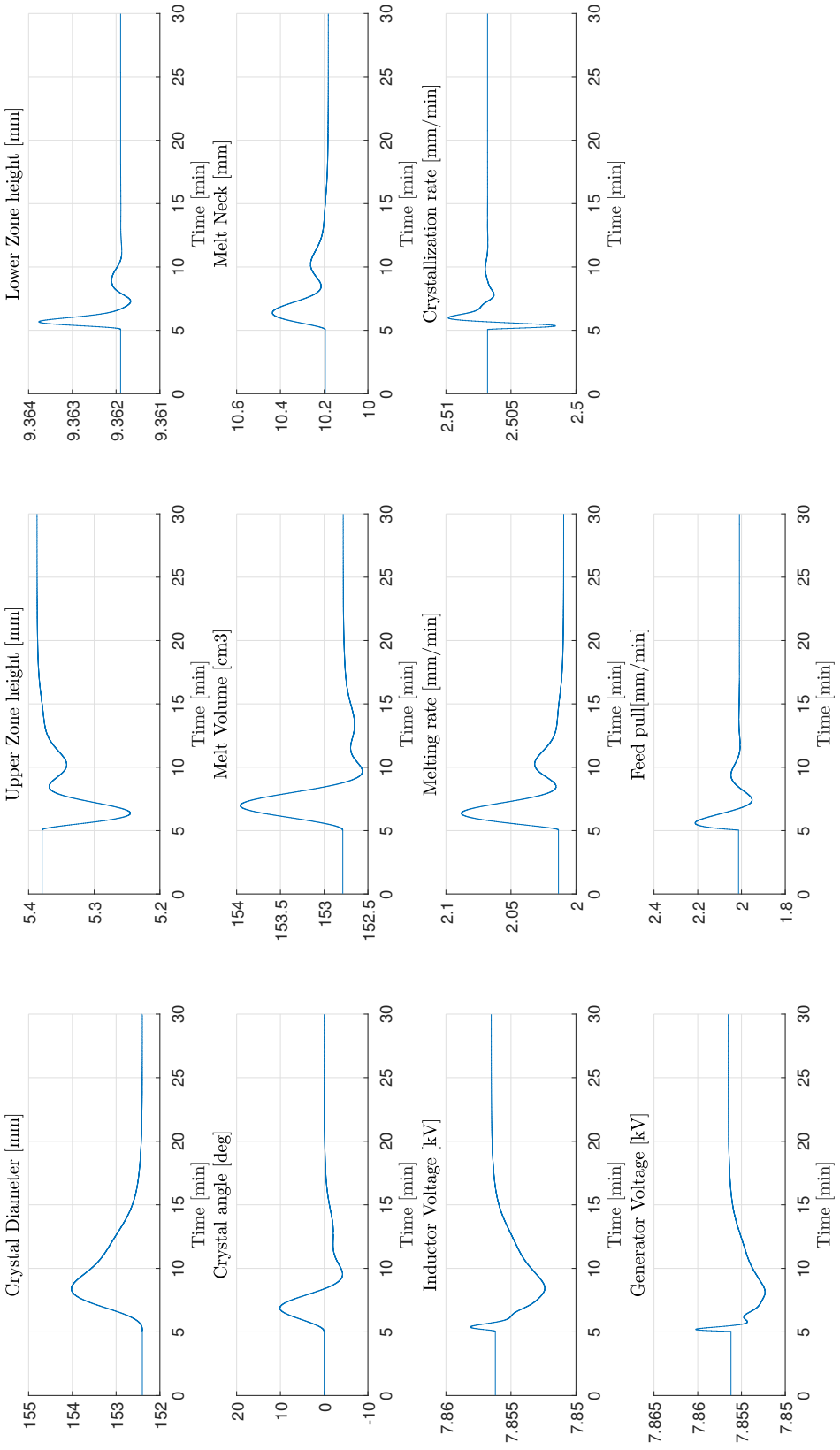

Figure 5: Figure of all states, with a disturbace in the diameter of the feed crystal

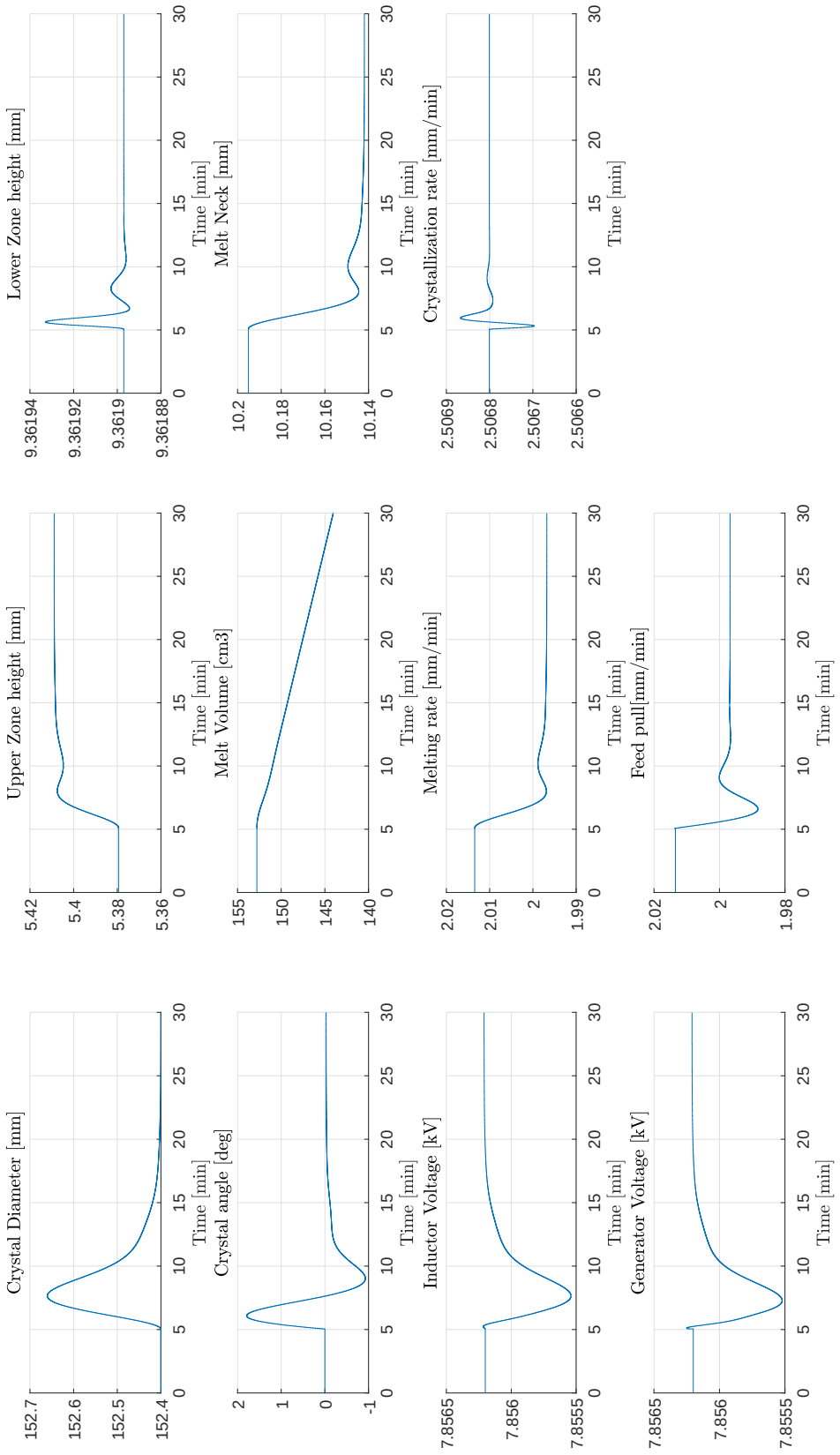

Figure 6: Figure of all states, with a model mismatch in the crystal angle